*Progress In Electromagnetics Research B, Vol. 61, 269–296, 2014*

# Finite Element Based Eigenanalysis for the Study of Electrically Large Lossy Cavities and Reverberation Chambers

**Constantinos L. Zekios, Peter C. Allilomes, Michael T. Chryssomallis, and George A. Kyriacou***

**Abstract**—An eigenanalysis-based technique is presented for the study and design of large complicated closed cavities and particularly Reverberation Chambers, including conductor and dielectric material losses. Two different numerical approaches are exploited. First, a straightforward approach is adopted where the finite walls conductivity is incorporated into the Finite Element Method (FEM) formulation through the Leontovich Impedance boundary conditions. The resulting eigenproblem is linearized through an eigenvalue transformation and solved using the Arnoldi algorithm. To address the excessive computational requirements of this approach and to achieve a fine mesh ensuring convergence, a novel approach is adopted. Within this, a linear eigenvalue problem is formulated and solved assuming all metallic structures as perfect electric conductors (PEC). In turn, the resulting eigenfunctions are post-processed within the Leontovich boundary condition for the calculation of the metals finite conductivity losses. Mode stirrer design guidelines are setup based on the eigenfunction characteristics. Both numerical eigenanalysis techniques are validated against an analytical solution for the empty cavity and a reverberation chamber simulated by a commercial FEM simulator. A series of classical mode stirrers are studied to verify the design guidelines, and an improved mode stirrer is developed.

## 1. INTRODUCTION AND MOTIVATION

The interest in the analysis and design of electrically large cavities is renewed during the last years, since interesting applications in reverberation chambers and auto-focused microwave cavities have been developed. However, all closed microwave cavities operate at their resonances and a small frequency band around them, while according to International Electrotechnical Commission (IEC) [1], a reverberation chamber should cover continuously a very wide frequency band from about 100 MHz to several GHz. Furthermore, the field distribution inside the chamber and especially over the region of the Equipment Under Test (EUT) should be homogeneous. Besides this, the use of reverberation chamber for electromagnetic compatibility testing and particularly for multiple-input-multiple-output (MIMO) antennas measurements constitute a very interesting and attractive application [2, 3].

As noted in [4] and became a common understanding, a critical aspect is the study of the mode stirrer's characteristics, a subject also explored in this work. To accomplish the desirable features one or more rotating stirrers are introduced inside the shielded enclosure. The role of the mode stirrer is to efficiently perturb-"stir" the resonant modes inside the chamber by varying the boundary conditions. Mode stirrers have been used for many years and there is also some research directed to the optimization of their design from Clegg et al. [5]. In the current work the stirrer's effects on the operation of the reverberation chamber is studied, where different mode stirrers are introduced and they are simulated varying their shape and size seeking for the appropriate one, according to IEC conditions.

*Received 18 July 2014, Accepted 22 October 2014, Scheduled 11 December 2014*

* Corresponding author: George A. Kyriacou (gkyriac@ee.duth.gr).

The authors are with the Microwave Laboratory, Department of Electrical and Computer Engineering, Democritus University of Thrace, Xanthi, GR 67100, Greece.

Most of the effort in the analysis and design of reverberation chambers is directed toward the solution of the deterministic electromagnetic problem (in the presence of specific sources). Method of Moments (MoM) is one of the most frequently used techniques for this type of problem in its simple form or extended by other techniques in a hybrid scheme [6–16]. Maybe the most complete work in this area is that of Bruns' [6, 7]. In [8–13], MoM is used with the aid of several techniques (spectral domain techniques [8], discrete singular convolution in a two dimensional analysis [9, 10], finite element boundary integral technique [12], MoM accelerated with Ewald and adaptive integral method [13]). However, in all these cases, the Perfect Electric Conductor (PEC) cavity Green's function is adopted, which is proved to be inaccurate, since it fails to account for the walls finite conductivity losses, neither can produce results for large objects in the cavity, and it is unable to model in detail a reverberation chambers (cables, screws, etc.). Moreover, the analysis of the stirrers in these works is simplified and is far from a realistic model, with the exception of [11]. Zhao introduces an integral equation accelerated by the Multi-Level Fast Multipole Method (MLFMM) in [14], but it is proved to be inappropriate for cavities since the specific technique is appropriate for far field, while the reverberation chamber requires near field. Two interesting works elaborate on the stirrer modeling [15, 16]. In [15], a 3D position stirring is shown, and a study of a simplified chamber is developed. Latter in [16], a simulation procedure is developed to show the relationship between the efficiency of stirring and the stirrer volume.

Further work in the simulation area of the reverberation chamber is based on a Finite Difference Time Domain (FDTD) analysis [17–20]. A full 3D simulation based on FDTD for independent positions of the stirrers has been established in [18]. In this work the simulation accounts for a large periodic antenna used to excite the chamber, and it presents the 3D simulation of the large reverberation chamber to reveal the independent positions of the stirrer. However, since a FDTD analysis is used in order to save computer resources maintaining the accuracy of the results, the introduction of unrealistically large losses is demanded. Additionally, FDTD techniques were unable to explicitly model the metallic walls finite conductivity, and the related losses are accounted through a controversial approximation assuming equivalent air volume Joule losses by a conductivity of $\sigma = 10^{-5}\,\mathrm{S/m}$. Moreover, the high quality factor of the chamber demands a long time range to be investigated. Specifically as referred in [18] in the time domain the simulation needs about $300,000$ times iterations, whereas in the frequency domain it needs a frequency step less than 1 MHz for the same investigation band. The eigenvalue analysis is superior from this point of view, since all the supported frequencies can be computed at once. A quite interesting work is [20] but only from the numerical point of view, since for the reverberation chamber analysis neither the efficiency of the stirrer nor the antenna is studied. Besides, the above FDTD adopted "staircase approximation" to model the stirrer paddles at its different positions-orientations, e.g., [18]. But it is well known that poor modeling of boundaries may cause significant shifts in eigenfrequencies, or even create pseudo modes that do not exist.

As a means to handle these problems it is herein proposed to employ a finite element based eigenanalysis approach, where the cavity resonant frequencies and corresponding quality factors comprise complex eigenvalues to be sought. Since eigenfunctions depend on the geometry and material loading but are independent of source type or location, the eigenanalysis can be carried out only once on the discretized geometry. In turn, only a small area around the specific source can be discretized, while an eigenfunction expansion can be utilized for the solution of the remaining large domain. The present effort constitutes the first step, namely eigenanalysis, toward this ultimate task. Our intention is to establish the FEM based eigenanalysis as a tool for the study of large cavities and the design and optimization of devices within that, especially mode stirrers, rather than an exhaustive analysis of reverberation chambers. The exploitation of eigenanalysis tools for specific design and optimization is left as a future task for any interested researcher.

Eigenanalysis of reverberation chambers has been studied in [21], and this is the most similar work to the one proposed herein, since a Finite Element Method (FEM) approach is also adopted. However, the work of Orjubin et al. [21] is restricted to the study of a reverberation chamber with the existence of only one non-realistic mode stirrer. Moreover, the frequency range concerns only the first modes of the RC, while a reverberation chamber is an overmoded cavity operating with more than 60 modes (usually 100–200 modes simultaneously exist). Finally in [21], an eigenanalysis is established but only for the linear case where neither metallic nor volume material losses are taken into account. In [22], the research group of Orjubin et al. have developed a Modal Distribution Analysis based on FEM. There a

wave chaos theory is used to study a modeled reverberation chamber, and the first 200 modes at a given stirrer position are determined. However, the mode stirrer in this work is again non realistic, since it consists of only two orthogonal paddles. Moreover, in [22] there is no consideration about the quality factor and the bandwidth of the excited modes.

There are a few attempts, e.g., [23] including our previous work [24] toward the employment of an eigenanalysis for the study and design of closed cavities, though in these works all cavity losses have been ignored. In our next work [25], cavity losses were taken into consideration, but this work presented only the main idea of how to treat large cavities. According to [2], the chamber amplitude calibration may be deduced from the current density flowing on its walls. In turn, these currents can be accurately obtained from the eigenvectors of the cavity when conductor losses are taken into account. Quality factor depends on both the dielectric losses of any object inside the cavity and the ohmic losses due to the finite wall's conductivity, and both of them are taken into account herein. The importance of the eigenanalysis for the study and design of reverberation chambers and particularly the required mode stirring is clearly identified by Rosengren and Kildal in their trend toward MIMO antenna measurements [4]. They explicitly stated that during their experimental work they experienced a large inaccuracy of measurements in the sub-band of 900–910 MHz. In turn, they found that this was due to a "hole in the mode distribution" where no mode was excited in this sub-band. Additionally, they explain that the "relative measurement accuracy goes as $1/\sqrt{N_m}$, where $N_m$ is the number of modes in each sub-band". Thus they conclude that "much larger frequency stirring is needed for uniform mode distribution with frequency" and hence uniform and acceptable measurements accuracy. These important observations clearly justify the necessity of the eigenanalysis and more importantly its exploitation in the mode stirrer analysis and design to achieve uniform frequency coverage. The original contribution of the present work falls exactly within this scope. In the work presented herein, an eigenanalysis is proposed where any losses are taken into account (finite conductivity of the metallic parts and/or losses of any material). Moreover, accounting for the mode stirrer study, a series of realistic models is introduced, and a full analysis of their efficiency and contribution in a wide frequency range (150 modes are determined) is analyzed. Furthermore, each introduced mode stirrer is rotated to observe its total functionality in the test area.

The finite element method (FEM) based on tetrahedral edge elements is adopted for the accurate formulation of the cavity eigenproblem. Dielectric losses are accounted through a complex permittivity (likewise any magnetic material losses through a complex permeability), while our first attempt to include finite conductivity losses from metallic walls and objects (mode stirrer, antenna scatterer, metallic supporting table) was toward a straightforward incorporation of the Leontovich impedance boundary conditions. This approach yields a non-linear, fourth-order polynomial eigenvalue problem. In order to solve this in principle non-linear eigenvalue problem, a linearization technique is applied. Indeed the straightforward "Leontovich approach" is proved to offer satisfactory results provided that a mesh size finer than about $\lambda/7$ is utilized for first-order edge elements providing a deviation of less than 4% in the resonant frequency (with respect to the analytical reference solution) and about 6% for the higher order modes quality factors. However, when complicated shaped mode stirrers with inclined blades are introduced in the cavity, a finer discretization reaching at least $500,000$ elements (half a million) is found necessary to ensure the same (or better) accuracy. In turn, the computer resources offered by a workstation (e.g., 64 core CPU with 256 GB of memory) were not adequate, and a computer cluster or graphics parallel processors (GPUs) should be employed [26]. But, instead of working toward this brute force direction, a more "clever" novel approach is devised.

Explicitly, the key idea was "implement the classical analytical approach based on PEC linear eigenproblem to estimate the finite conductivity metallic losses". We have already published the idea itself in [27], while herein this methodology is exploited in the study of practical electrical large closed structures. An eigenproblem based on the solution of the electric and/or magnetic field wave equation is formulated. Both approaches are implemented and are proved to be robust providing an accuracy better than 4% fulfilling all practical necessities. Besides that, these PEC approaches were able to simulate on a simple computer all chambers including the most complicated mode stirrers, supporting tables and EUT models.

Mode stirrer design guidelines are also devised to be used as a rule of thumb. Explicitly, the field uniformity requirements as set by IEC [1] can be reliably fulfilled by rotating mode stirrers of appropriate

shape. According to Clegg et al. [5], although mode stirrers are used for many years, there has been very little research on their modeling and particularly into their shape optimization. The aims setup when mode stirrers are utilized is to transform the chamber discrete operating frequency spectrum (field exists only within a small bandwidth around each resonance) to a "continuous" as far as possible, along with the achievement of energy and polarization uniformity over the testing area. Working toward this direction, a step-by-step approach is followed by which the proposed "design guidelines" are verified, where we start from a simple shaped mode-stirrer and move toward more complicated geometries. These discrete steps are defined so that each one verifies one of the guidelines, while finally all of them are combined. Note that the present effort is not directed toward the exhaustive design of a particular reverberation chamber. The scope is rather to prove how an eigenanalysis tool can serve this purpose focusing on the mode stirrers and encourage Engineers to exploit eigenanalysis tools in the study and design of arbitrary loaded large cavities or chambers.

## 2. FORMULATIONS AND EQUATIONS

The simplified topology of the problem shown in Figure 1 is considered at the first steps. It is a closed metallic cavity containing an antenna, the EUT and a metallic mode stirrer. All the cavity's walls, the stirrer's the antenna's and the EUT's walls are assumed to have finite conductivity.

The whole structure including the objects' perturbing the cavity is simulated using FEM, employing edge elements. Aiming at a general formulation, an arbitrarily shaped three-dimensional computational domain $V$ inhomogeneously loaded with an in general anisotropic material is assumed. Its electromagnetic behavior can be characterized by the electric field vector wave equation, which is described with the aid of tensor permittivity ($\bar{\bar{\epsilon}}_r$) and permeability ($\bar{\bar{\mu}}_r$) and in the absence of any exciting source, reads:

$$\bar{\nabla}\times\bar{\bar{\mu}}_r^{-1}\cdot\bar{\nabla}\times\bar{E} - k_0^2\bar{\bar{\epsilon}}_r\bar{E} = 0 \tag{1}$$

Applying a standard Galerkin procedure, the following weak formulation can be derived, e.g., [28]:

$$\iiint_V (\bar{\nabla}\times\bar{T})\cdot\bar{\bar{\mu}}_r^{-1}\cdot(\bar{\nabla}\times\bar{E})dV - k_0^2\iiint_V \bar{T}\cdot(\bar{\bar{\epsilon}}_r\bar{E})dV - jk_0\iint_S \bar{T}\cdot(\hat{n}\times\bar{H})dS = 0 \tag{2}$$

where $\bar{T}$ is the test function and is chosen according to Galerkin's procedure to be equal to the function that describes the electric field. Moreover, since the solution domain involves vector fields, the test functions are vector functions, and the corresponding elements are the popular set of "edge elements". A full description of the form of these functions used herein can be found in any technical book of finite elements for electromagnetics, e.g., [28, Chapter 2.5.2.1] or in [29]. $V$ defines the integration at the volume domain and $S$ the integration over the surfaces of the structure. The surface integral is

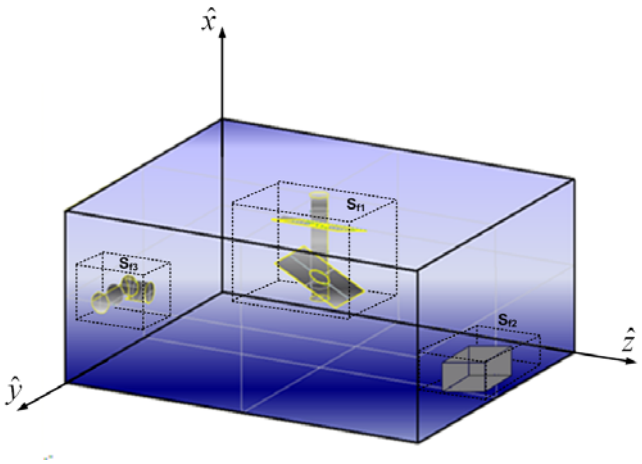


**Figure 1.** A simplified reverberation chamber model comprised of an inhomogeneously loaded cavity with the antenna the EUT and the metallic mode stirrer.

defined over the surface enclosing the solution domain (cavity walls) as well as on the surface of any object existing within the cavity. It is through this integral that general impedance boundary conditions are enforced within the FEM formalism. Specifically this integral serves to introduce conductor losses, according to the Leontovich boundary condition:

$$\hat{n}_k \times \left(\hat{n}_k \times \bar{E}\right) = Z_S \left(\hat{n}_k \times \bar{H}\right) \tag{3}$$

$Z_S$ is the surface impedance of the form [28]:

$$Z_S = (1+j)\sqrt{\frac{\omega\mu_0}{2\sigma}} = (1+j)\sqrt{k_0}\sqrt{\frac{\mu_0 c}{2\sigma}} \tag{4}$$

where the metallic walls are considered non-magnetic with $\mu = \mu_0$, $\sigma$ their conductivity, and $c$ the speed of light.

Substituting condition (3) in the formulation and taking into consideration the fact that the inward unit vector is $\hat{n}_k = -\hat{n}$, Eq. (2) becomes:

$$\iiint_V \left(\bar{\nabla} \times \bar{T}\right) \cdot \bar{\bar{\mu}}_r^{-1} \cdot \left(\bar{\nabla} \times \bar{E}\right) dV - k_0^2 \iiint_V \bar{T} \cdot \left(\bar{\bar{\epsilon}}_r \bar{E}\right) dV - jk_0 Z_0 \iint_S \frac{1}{Z_S} \bar{T} \cdot \left[\hat{n} \times \left(\hat{n} \times \bar{E}\right)\right] dS = 0 \tag{5}$$

The resulting system of equations is in turn formulated into a nonlinear generalized eigenvalue problem by separating the terms involving the free space wavenumber $k_0$ (or the circular frequency $\omega$, as $k_0 = \omega/c$). The final matrix form can be formulated as a nonlinear eigenvalue problem for the unknown resonant wavenumber (eigenvalues $k_0$) as:

$$[S_{el}][e] - k_0^2[T_{el}][e] - j\sqrt{k_0}[L_{el}][e] = 0 \tag{6}$$

$$[S_{el}] = \iiint_V \left(\bar{\nabla} \times \bar{T}\right) \cdot \bar{\bar{\mu}}_r^{-1} \cdot \left(\bar{\nabla} \times \bar{E}\right) dV \tag{7}$$

$$[T_{el}] = \iiint_V \bar{T} \cdot \left(\bar{\bar{\epsilon}}_r \bar{E}\right) dV \tag{8}$$

$$[L_{el}] = Z_0 \iint_S \frac{1}{Z_S} \bar{T} \cdot \left[\hat{n} \times \left(\hat{n} \times \bar{E}\right)\right] dS \tag{9}$$

where $[e]$ is a vector composed of the electric field values at the middle of element's edges.

The polynomial eigenvalue problem obtained above in (6) can be solved using symmetric or companion linearization, described next in Subsection 2.3.

From a physical point of view, the reverberation chamber is a closed electromagnetic cavity containing a number of relatively small objects which perturb its characteristics. Specifically as a closed cavity, electromagnetic field inside it exists only at discrete resonant frequencies and at a small bandwidth around them which is defined by each mode quality factor. The presence of the static objects (antenna and EUT) causes a shift of this discrete spectrum. Additionally, the purpose of a rotating mode stirrer is to "spread these frequencies" by producing different shift for each angular orientation so as to cover almost continuously the whole chamber operating frequency band. Simultaneously, the variation of these resonant frequencies is accompanied by a change in their modal field (eigenfunctions) distributions, which aims at providing a field as uniform as possible over the test area. Obviously, the reference structure for both the resonant frequencies and their eigenfunctions is the empty rectangular cavity. Thus it is useful to present a short review of its characteristics along with the related quality factors. Based on this analysis, the guidelines for the mode stirrer design and an efficient way of calculating the quality factor of a simulated practical cavity (even of arbitrary shape) will be given next.

### 2.1. Modal Fields of PEC Rectangular Cavity

The modal fields of a rectangular cavity with perfect electric walls (PEC) is well known through an analytical solution by the separation of variables. As it is well known for a homogeneously filled (or empty) cavity, the *TE* and *TM* modes are uncoupled and constitute an orthogonal basis which is orthonormal in the absence of mode degeneration, or when each mode has a unique resonant frequency,

e.g., Lehman [30]. The electromagnetic field generated by any source can be expanded into a sum of these modal fields. The modal field expressions for a uniformly filled rectangular cavity are available in classical textbooks, e.g., [31, 32] and are also given in Appendix A in a convenient form.

The dispersion condition resulting from the separation of variables is:

$$k^2 = k_x^2 + k_y^2 + k_z^2 = \left(\frac{m\pi}{a}\right)^2 + \left(\frac{n\pi}{b}\right)^2 + \left(\frac{l\pi}{d}\right)^2 = \omega^2\mu\epsilon \tag{10}$$

where $m$, $n$, $l = 0, 1, 2, \ldots$, but $m \neq 0$, $n \neq 0$ for $TM_{mnl}$ modes and $l \neq 0$ for $TE_{mnl}$ modes. The resonant frequency of the cavity can be easily calculated:

$$f_{r_{mnl}} = \frac{c}{2\pi\sqrt{\mu_r\epsilon_r}}\sqrt{\left(\frac{m\pi}{a}\right)^2 + \left(\frac{n\pi}{b}\right)^2 + \left(\frac{l\pi}{d}\right)^2} \tag{11}$$

The solution above is satisfied only in the case of the empty PEC cavity or in the case that is homogeneously filled with an isotropic material. Even though the PEC wall analytical expressions are very useful, ignoring losses for an empty cavity is equivalent to presume an infinite quality factor or zero modal bandwidth, which is far from the practical situation. However, an approximate evaluation of losses due to finite conductivity walls is classically possible and this will be recalled next in an abstract form.

### 2.2. Definition of Quality Factor

For a theoretical cavity of perfect electric conductive walls, the spectral response of each mode is just an impulse (delta function). In contrary, for a real cavity of finite conductivity, each mode resonance spreads in a frequency band $\Delta f_Q$ inversely proportional to the the quality factor of the cavity $\Delta f_Q = f_0/Q$. As it occurs the quality factor estimation is of significant importance, since a high value describes a chamber of low losses at the specific frequency and the ability to store high levels of energy, but at the expense of smaller operating bandwidth around each resonance.

In general, the quality factor is calculated from the field distribution inside the cavity using the equation:

$$Q = \omega \cdot \frac{\text{average energy stored}}{\text{Power losses}} = \omega \cdot \frac{W_m + W_e}{P_l} \tag{12}$$

where $W_m$ and $W_e$ are the magnetic and electric stored energy respectively, e.g., [33, Page 390]. The power dissipated in any good conductor is classically known as the Joule losses (proportional to $\bar{J} \cdot \bar{E}$), hence the same principle applies to the finite conductivity cavity walls as well as for any metallic object inserted in the cavity. The material losses (objects in the cavity) are accounted through the imaginary parts of the permittivity ($\epsilon = \epsilon' - j\epsilon''$) and the permeability ($\mu = \mu' - j\mu''$). The totally dissipated power, due to material losses, reads:

$$P_l = \frac{1}{2}\oiint_S \bar{J} \cdot \bar{E}^* dS + \frac{\omega}{2}\iiint_V \left(\epsilon''\bar{E}^2 + \mu''\bar{H}^2\right) dV \tag{13}$$

Equation (13) is general and can be used whenever the electric and magnetic fields within the cavity are available either from an analytical or a numerical solution. However, even for an empty cavity the boundary conditions on a finite conductivity wall are complicated, depend on frequency (dispersion) and are known as impedance conditions. A good approximation usually adopted is that of Leontovich given in Equation (3). But, the main difficulty with (3) is that it introduces a coupling across the walls between the electric and the magnetic field. Hence, even for an empty or homogeneously filled cavity the electric and the magnetic field wave equations cannot be exactly solved separately. Correspondingly, there are not pure $TE$ and $TM$ modes any more but those become hybrid. An exact analytical solution is in turn very difficult and requires sophisticated techniques or a numerical approach. However, this coupling effect is proved to be a local phenomenon restricted around the finite conductivity conductors, while away from them the $TE$ and $TM$ mode eigenfunctions are retained. A very rough approximation calculates the finite conductivity losses considering this local phenomenon as a plane wave incident on the metallic walls. This yields a simplified expression often used in practice [6], which does not discriminate

between different modes. An approach providing each mode quality factor with a sufficient accuracy is based on the modal field evaluated analytically considering PEC walls (ignoring metallic losses). This approach was recently proved to perform impressively well for arbitrarily shaped cavities by utilizing numerical eigenfunctions which are calculated assuming PEC metallic surfaces [27]. Besides these approximations, including the conductor losses within the formulation requires a numerical solution of the resulting non-linear eigenvalue problem, but it yields the true eigenfunctions and the related accurate quality factors.

### *2.2.1. Practical Estimation of the Quality Factor*

The IEC proposed quality factor approximation for rectangular reverberation chambers in [1] is:

$$Q_{\text{IEC}} = \frac{3V}{2\mu_r \delta_s A} \frac{1}{1 + \dfrac{3\lambda}{16}\left(\dfrac{1}{a} + \dfrac{1}{b} + \dfrac{1}{d}\right)} \tag{14}$$

where $V$ is the structure's volume, $a$, $b$, $d$ the cavity's dimensions, $A$ the area of the reverberation chamber's inner surface while $\delta_s$ is the skin depth:

$$\delta_s = \frac{1}{\sqrt{\pi f \mu \sigma}} \tag{15}$$

Formula (14) has a little practical use, since the resulting $Q$ values are proved to be inconsistently too high by a factor of 10–500, compared with measurements according to [6].

### *2.2.2. PEC versus Exact Non-Linear Eigenproblems*

The finite wall conductivity can be considered as a perturbation of the corresponding PEC situation, and the respective eigenfunctions can be utilized as fair approximations. But again to evaluate losses from (13) we need both the electric and the magnetic fields tangential to the wall, where (3) should apply. Recall now that the required tangential electric field was enforced to vanish across the PEC wall, hence it is not available. Explicitly, the PEC and PMC (Perfect Magnetic Conductor) boundary conditions read:

$$\hat{n} \times \bar{E} = 0 \quad \& \quad \hat{n} \cdot \bar{H} = 0 \quad \rightarrow \quad \text{PEC} \tag{16}$$

$$\hat{n} \times \bar{H} = 0 \quad \& \quad \hat{n} \cdot \bar{E} = 0 \quad \rightarrow \quad \text{PMC} \tag{17}$$

It seems that we are at a dead-end, but a new approximation is again proved valid. Explicitly, the normal magnetic field at the surface of a PEC is zero as in (16), but the tangential magnetic field becomes maximum, as also denoted by the cosine dependencies in (A4), (A6), (A10) and (A12). Hence the relatively small change in the tangential magnetic field caused by substituting PEC with a finite conductivity wall will be negligible. The same is also true for the current density flowing on the finite conductivity wall which can be assumed approximately equal to the corresponding surface current density flowing on the PEC wall and is defined by $\bar{H}_{\tan}$ as:

$$\bar{J} = \bar{J}_S = \hat{n} \times \bar{H}_{\tan} \tag{18}$$

Actually, a current sheet with a homogeneous density is assumed to flow up to a thickness equal to a skin depth. In contrary, a similar change in the zero for PEC tangential electric and normal magnetic field would be very significant (Figure 2). Now, with the availability of a good approximation for $\bar{H}_{\tan}$ (Figure 2(b)) the desired $\bar{E}_{\tan}$ can be calculated through (3) which can be also written as:

$$\bar{E}_{\tan} = Z_S \left(\hat{n} \times \bar{H}_{\tan}\right) \tag{19}$$

Substituting (18) and (19) into the first term of (13), the conductor losses ($P_{LC}$) can be estimated solely through the tangential magnetic field from the eigensolution with PEC walls obtained either analytically or numerically as:

$$P_{LC} = \frac{R_s}{2} \oiint_S \left|\bar{H}_{\tan}\right|^2 dS \tag{20}$$

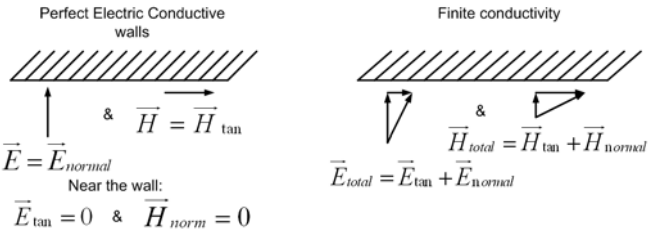


**Figure 2.** Electric and magnetic boundary conditions over a metallic wall with (a) infinite and (b) finite conductivity.

where $\bar{H}_{\tan} = \bar{H}^{PEC}_{\tan} = \bar{H}^{PEC}$ since $\bar{H}^{PEC}_{norm} = 0$ across the PEC wall. Regarding the second term of (13), the involved electric and magnetic fields are basically defined at an adequate distance away from the metallic objects, hence they can be approximated by the fields of the eigensolution with PEC walls ($\bar{E} = \bar{E}^{PEC}$, $\bar{H} = \bar{H}^{PEC}$). Thus the total cavity losses are approximately given by:

$$P_l = \frac{R_s}{2} \oiint_S \left|\bar{H}^{PEC}\right|^2 dS + \frac{\omega}{2} \iiint_V \left(\epsilon'' \left|\bar{E}^{PEC}\right|^2 + \mu'' \left|\bar{H}^{PEC}\right|^2\right) dV \tag{21}$$

The analysis presented above yields very important conclusions:

- The modal eigenfunction of a practical loaded cavity are approximately the same with those obtained from the eigenproblem with PEC walls and PEC metallic objects. These can be exploited for the evaluation of:
  - The magnetic $W_m$ and electric $W_e$ stored energy.
  - Both the conductor and material losses through (21).
  - The modal quality factors substituting these quantities into (12) or recalling that at resonance $\omega = \omega_0$ the energy oscillates (one maximized the other vanishes and vice-versa) in time between its electric and magnetic form as $W_e(\omega_0) = W_m(\omega_0)$, then (12) reads:

$$Q_0 = \frac{2\omega_0 W_e(\omega_0)}{P_L} = \frac{2\omega_0 W_m(\omega_0)}{P_L} \tag{22}$$

Even though classical knowledge is utilized in the above reasoning, a very important conclusion is extracted as: *"There is no practical need to solve the eigenproblem including the non-linear metallic conductor losses, but all necessary quantities can be approximately extracted from the PEC eigenmode solution"*. This is a great simplification since the PEC eigenproblem is linear, while when conductor losses are included through Leontovich impedance conditions it becomes non-linear of fourth order involving $\sqrt{k_0}$ and $k_0^2$. Solving a linear eigenproblem directly yields the whole eigenspectrum, while the non-linear one requires sophisticated techniques usually based on initial values of a related linear configuration which are iteratively updated. If a non-linear eigenproblem is inevitable, it is preferable to adopt linearization techniques applicable to polynomial forms, and this approach is followed next. Such an inevitable practical case can be any heavily loaded cavities with large metallic objects or relatively electrically small cavities.

### 2.3. Numerical Solution of the Non-Linear-Eigenproblem

In order to solve numerically the Polynomial Eigenproblem (PEP), a transformation into a linear Generalized Eigenproblem (GEP) of larger size ($mxn$) is applied herein. In general, there are two main linearization techniques, the companion and the symmetric, but they are not unique for the given problem. The companion linearization is the mostly used in practice, even though it leads into a non-positive definite matrix constituting a serious problem for the solution procedure. For the case of the symmetric linearization, there is a lack of GEP techniques that can be applied directly. The standard direct solver fails to manipulate this problem not only due to its size but also due to its ill-conditioning. The main difficulty in the direct solver is the inversion of the right-hand side matrix since its determinant

vanishes. Thus, the only alternative is the use of iterative solvers, which are in general most efficient especially for large sparse systems of this order, for instance Arnoldi or Jacobi-Davidson technique. The problem herein is the type of factorization deflation. Most iterative solvers use a Cholesky factorization, for complex eigenvalue systems, in order to bring the system in an appropriate form before applying the iterative technique and solve it. Because in "Leontovich problem" the linearized matrices are not positive definite, the Cholesky factorization cannot be constructed. This obstacle can only be overcome using an iterative algorithm with a different kind of factorization. The solution procedure we use is an initial QR factorization and in turn an Arnoldi algorithm with a specific sigma shift, which exploits the sparsity of the matrix system [34].

Examining the form of (6), the polynomial eigenvalue problem can be transformed into an equivalent fourth-order linear problem using a linearization technique defined as eigenvalue transformation.

*2.3.1. Eigenvalue Transformation*

The form of (6) can be easily characterized as a fourth-order eigenvalue problem, by simply setting $\sqrt{k_0} = \lambda$. Thus it can be written in a more general form as:

$$\Psi(\lambda) = \lambda^4 \cdot C_4 + 0 \cdot C_3 + 0 \cdot C_2 + \lambda \cdot C_1 + C_0 = 0 \tag{23}$$

where $C_4 = -T_{el}$, $C_1 = jL_{el}$ and $C_0 = S_{el}$. After the companion linearization the form obtained becomes:

$$A[e] = \lambda B[e] \tag{24}$$

where:

$$A = \begin{bmatrix} 0 & I & 0 & 0 \\ 0 & 0 & I & 0 \\ 0 & 0 & 0 & I \\ -S_{el} & -jL_{el} & 0 & 0 \end{bmatrix} \quad \text{and} \quad B = \begin{bmatrix} I & 0 & 0 & 0 \\ 0 & I & 0 & 0 \\ 0 & 0 & I & 0 \\ 0 & 0 & 0 & -T_{el} \end{bmatrix} \tag{25}$$

The solution procedure of this kind of problem produces two pairs of complex conjugate eigenvalues of the form:

$$\lambda_i = \pm\lambda_i' \pm j\lambda_i'' = |\lambda|\, e^{j\theta} \tag{26}$$

Only positive eigenvalue with both real and imaginary positive values can be accepted as representing physical resonant modes. An eigenvalue with negative real part (negative resonant frequency) has no physical meaning and can only be defined as an image of the corresponding positive in frequency domain. The desired complex wavenumber is then calculated as:

$$k_0 = \lambda^2 = |k_0| e^{j\theta_0} \quad \rightarrow \quad |k_0| = |\lambda|^2, \quad \theta_0 = 2\theta \tag{27}$$

## 3. MODE STIRRER DESIGN-GUIDELINES

Electromagnetic field in closed cavities exists only at specific resonant conditions-modes, at which constructive (in-phase) interference of the multiply reflected waves from its walls and any enclosed objects (perturbations) occurs. These set up standing waves in each direction and thus resulting in field-energy maxima and minima at different locations for each mode. Besides that according to [4] each mode can be described as a superposition of eight plane waves (four when one mode indice is zero) incident on the EUT from a different angle. Thus ensuring the excitation of multiple modes and placing the EUT at a location where they exhibit significant field intensity may ensure the fulfilling of amplitude and polarization requirements. The utilization of the mode stirrer aims exactly at the excitation of multiple resonating modes so that at each point of the area, where the EUT will be located, field components at all possible polarizations (directions) exist, while the related energy should be almost equal (within 1 dB deviation) when averaged in time. Attaching metallic scatterers on the rotating axis of the mode stirrer the maxima and minima of the field-energy can be appropriately exploited, producing a homogeneous field inside the reverberation chamber. In the course toward the establishment of some design principles, the interaction of a metallic scatterer with a field incident on that should be recalled, as follows: i) For a scatterer to interact it should be located in an area where the field is not minimum, and the phenomenon becomes more intense as the scatterer passes-moves

through region of field maximum. ii) From basic boundary conditions the field interaction-reflection is maximized when the electric field is parallel to the metallic scatterer and is minimized when it becomes perpendicular. iii) The presence of the metallic scatterer changes the resonant conditions regarding both the resonant frequency and the corresponding quality factor (and the related bandwidth) as well as the modal field distribution (eigenfunctions). Keeping the above in mind and exploiting the knowledge of the canonically shaped analytically available modal fields (eigenfunctions) some design guidelines for the mode-stirrer design are extracted and verified herein.

The location of the whole mode stirrer is presumed by the practical measurement configuration as shown for the example in Figure 1. Thus, the chamber base (floor) should be freely accessed by

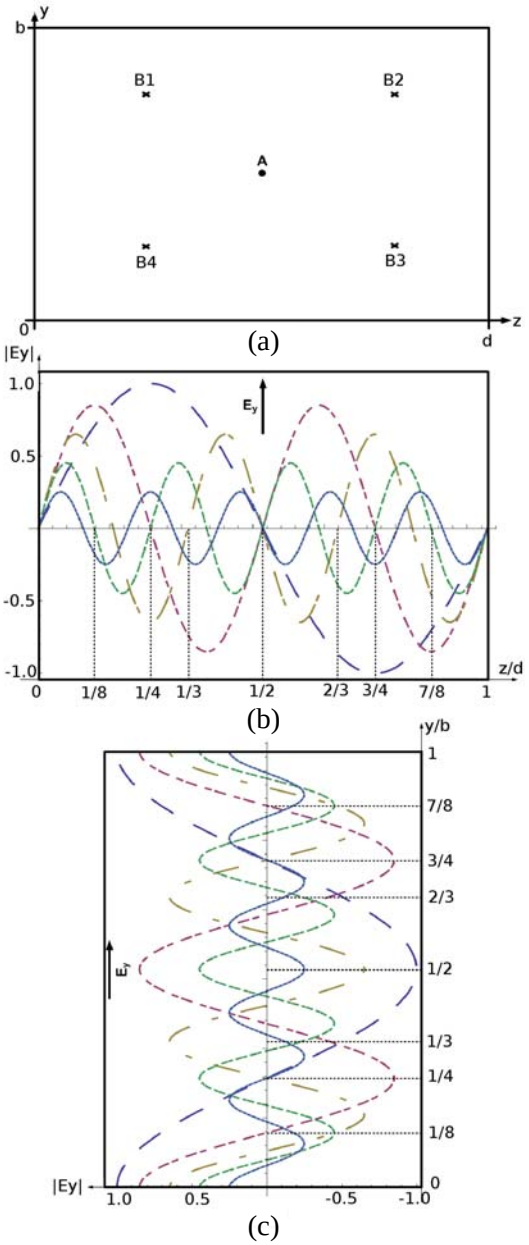


**Figure 3.** (a) Possible modes stirrer locations on the horizontal cross-section, (b) sinusoidal eigenmode field distributions for electric components parallel to PEC walls, (c) cosinusoidal eigenmode field distribution for electric components normal to PEC walls. Note that modes are depicted with different amplitudes only for viewing convenience.

the personnel, and the location of the source (transmitting antenna) and the testing area (location of Equipment Under Test, EUT) should be defined across it. Hence, the mode stirrer should be hanged from the ceiling, and due to its required large size it is more appropriate to be located at the midpoint (A location in Figure 3(a)), but other locations are also utilized. Additionally, the one quarter locations marked as $B_1$–$B_4$ in Figure 3(a) can be good candidates for smaller possibly multiple scatterers or "distributed" scatterers. Another question concerns the height of the mode stirrer (or its distance from the top wall-roof). For the appropriate selection, the electromagnetic point of view should be adopted.

The modes excited in the empty cavity are classified as $TE^z_{mnl}$ (with $E_z = 0$) and $TM^z_{mnl}$ (with $H_z = 0$), where the subscripts $(m, n, l = 0, 1, 2, \ldots, \infty)$ correspond to the number of half wavelengths contained in the cavity dimensions ($a$, $b$, $d$) respectively. Focusing on the electric field components since perfect electric (metallic) scatterers are considered, the $E_y$ component retains sinus dependence in the $z$-direction and cosinus dependence in the $y$-direction as shown in Figures 3(b), (c). The $E_z$ dependence is exactly vice-versa. Both $E_z$, $E_y$ are parallel to the $x = 0$, $a$ walls, and thus they present sinus behavior along the height $a$. Conversely, the $E_z$ component appearing only in the $TM^z$ modes behaves as sinus in the $x$- and $y$-directions and cosinus in the $z$-direction.

Keeping the above in mind and particularly the form of distributions in Figures 3(b) and 3(c), one may observe that placing a scatterer parallel to the $(yz)$ plane at points around $B_1$–$B_4$ (Figure 3(a)) with length at least $d/8$ (assume $d > b$) can effectively disturb $E_z$, $E_y$ components, provided that these scatterers are appropriately located across the height $a$-dimension. Note that placing thin scatterers at all four $B_1$–$B_4$ positions is wrong, since these will act like an effective wall restricting the chamber height and increasing all the resonant frequencies. Assuming for example a chamber with dimensions $a = 0.2\,\text{m}$, $b = 0.4\,\text{m}$, $d = 0.5\,\text{m}$ and placing the four plane scatterers at a height $a' = 3a/4$, the well-known resonance Formula (11) yields for the indicative $TE^z$-modes $(m, n, l) = (1, 0, 1)$, $(0, 1, 1)$, $(1, 1, 1)$ an increase in resonant frequencies from $(480, 808, 891)\,\text{MHz}$ to $(548, 850, 929)\,\text{MHz}$ or an upward shift by $(14, 5, 4.3)\%$ respectively. This will be a very undesired effect since a significant part of the low operating frequencies band will disappear. On the contrary, by placing only one scatterer and rotating it around, the same field disturbance will be achieved, but both the original resonating heights $a$ and disturbed $a'$ will be preserved, and thus resonant modes around both the unperturbed and perturbed sets will be sustained. Actually, the presence of the metallic axis holding the scatterer (as well as the scatterer itself) will cause a decrease in resonant frequencies from those of the empty cavity, similar to that observed going from an empty cylindrical to a coaxial cavity. Returning to $E_z$, $E_y$ distribution along-$a$ is similar to Figure 3(b) thus presenting minima at distances $a/3$, $a/4$, $a/5$ from the roof wall, at which the placement of thin scatterers should be avoided. Instead again of multiple scatterers, it seems preferable to introduce a slant scatterer forming an angle (e.g., $60^\circ$) with the vertical axis (e.g., Figures 10, 13). In this manner, field disturbance along a range of heights can be caused, but this scatterer can also perturb the $E_x$ component.

Summarizing the above discussion a single slant oriented with respect to $x$-axis (or multiple as in Figure 10) thin metallic scatterer effectively disturbs all $E$-field components and thus changing the field distribution and the resonant frequencies. Additionally, a large metallic structure should be avoided as it effectively "short circuits" a large volume. At the same time, it is very important to cause a large perturbation in the low order resonant modes which are more sparse than the high order modes. Thus, to adopt multiple horizontal or slant scatterers at different appropriate heights with significant angular distance between them, but with relatively small width in order to retain the full height resonating lengths.

## 4. NUMERICAL STUDY OF MODE STIRRERS

A reverberation chamber with dimensions 2 m, 4 m, 5 m and metallic walls of finite conductivity ($\sigma = 58 \cdot 10^6\,\text{S/m}$) is examined. The scope of the simulation procedure refers to the stirrer's effects on the resonant frequency spectrum, which is the only changing-rotating perturbation inside the chamber, thus the relative permittivity and permeability of air is considered. As noted in [4] and discussed in the introduction, the examination of the modal eigenspectrum to ensure that there are no holes-gaps is of critical importance for the accuracy of antenna measurements. A simulation set of five mode stirrers is introduced presenting its shape effects on the resonances. Both the geometry design capture

and the mesh initialization are achieved using the free open source program SALOME [35], while the presented numerical technique has been developed and incorporated in the collection of the free software FEniCS [36]. In order to repeat the presented results, for the interested reader, a brief description is given below for the simulation procedure.

The free open source program SALOME is used for both the design and mesh initialization of the studied geometry. In the *Computer Aided Design* (CAD) environment, the structure is designed, and each region is characterized according to its material features. Moreover, the surfaces are defined as either perfect electric conductors or conductors of finite conductivity according to the problem's demands. In turn, the *Mesh* environment is activated where the designed structure is discretized. Since edge vector elements are used for the problem formulation [29], the structure is discretized by tetrahedrals and triangles in the inner and surface domain, respectively. After the mesh initialization a file of ".med" type ([35]) is exported, which is organized in ".hdf5" format [37]. A parsing module has been developed to interpret the ".hdf5" file into ".xml" format [38]. This ".xml" file contains all the necessary information of the mesh file. After that, using our in-house developed code through FEniCS, the problem is formulated according to Eq. (2). To solve the problem, a shift and invert Arnoldi algorithm is used, where the following parameters are set: The problem type which is of non-hermitian type, the spectral shift which is according to the desired eigenvalues (here the spectral shift is the normalized resonant wavenumber which belongs into the region $k_r \in (1.0, 5.0)$), the number of desired eigenvalues and the corresponding eigenvectors to compute (here is set to 200) and finally the error tolerance (here is set $\approx 10^{-8}$). To replicate the stirrers, the geometrical characteristics of each one are given in detail in Figures 4, 7, 10, 13, and 16.

### 4.1. Numerical Validation Test

For the first attempt, the reverberation chamber is modeled using 450 elements as an empty cavity in the absence of any structure inside. The eigenvalues are presented in Table 1 along with the PEC walls analytic solution for the ten first resonant modes. It is well understood that the number of calculated eigenvalues depends on the rank of the matrix which is defined by the spatial sampling. Herein, a discretization resolution better than $\lambda_{\min}/3$ is always ensured, resulting in more than 150 calculated complex eigenfrequencies. But it was observed that studying the 10 first modes, one can have a very good idea of the structure behavior. Thus, the first 10 modes are depicted in the following tables for convenience, although the whole eigen-spectrum is stored for later processing. The percent deviation is always less than 2.5%. In this case, the quality factor is infinite, since PEC walls are assumed. The first computation of the quality factor is achieved by accounting for the empty cavity copper walls losses with the aid of the FEM algorithm which incorporates the Leontovich boundary conditions within the formulation, denoted from now on as "Leontovich-FEM". The discretization resolution $\Delta l$ should

**Table 1.** Computed resonant frequencies (both ours and HFSS) of an empty cavity with PEC walls versus their analytical values.

| | Mode | Analytical MHz | FEM MHz | HFSS MHz | Relative Error % |
|---|---|---|---|---|---|
| 1 | $TE_{011}$ | 48.0 | 47.8 | 47.8 | 0.417 |
| 2 | $TE_{012}$ | 70.8 | 69.8 | 70.2 | 1.412 |
| 3 | $TE_{021}$ | 80.8 | 79.2 | 80.5 | 1.980 |
| 4 | $TE_{101}$ | 80.8 | 80.7 | 80.5 | 0.124 |
| 5 | $TM_{110}$ | 83.9 | 83.5 | 83.5 | 0.477 |
| 6 | $TM_{111}$ | 89.1 | 88.3 | 88.5 | 0.899 |
| 7 | $TE_{111}$ | 89.1 | 89.6 | 88.5 | −0.561 |
| 8 | $TE_{022}$ | 96.0 | 93.7 | 94.0 | 2.396 |
| 9 | $TE_{102}$ | 96.0 | 94.2 | 94.0 | 1.875 |
| 10 | $TE_{013}$ | 97.5 | 96.0 | 97.0 | 1.538 |

**Table 2.** Quality factor of the empty cavity with copper walls calculated by "Leontovich-FEM", "PEC-FEM" and HFSS versus their analytical values, Eq. (12).

| | | | "Leontovich-FEM" | "PEC-FEM" 2733 el. | HFSS | rel. err. % | |
|---|---|---|---|---|---|---|---|
| | Mode | Anal. | 24173 el. | $E$-field | 350 high. ord. el. | leont/ analytical | $E$-field/ analytical |
| 1 | $TE_{011}$ | 109096 | 108738 | 108916 | 109062 | 0.328 | 0.165 |
| 2 | $TE_{012}$ | 137114 | 136055 | 136736 | 136942 | 0.772 | 0.276 |
| 3 | $TE_{021}$ | 116487 | 116423 | 116780 | 116341 | 0.055 | −0.252 |
| 4 | $TE_{101}$ | 137870 | 136771 | 137369 | 137673 | 0.797 | 0.363 |
| 5 | $TM_{110}$ | 125939 | 125779 | 126049 | 125776 | 0.127 | −0.087 |
| 6 | $TM_{111}$ | 109821 | 109823 | 111600 | 104738 | 0.002 | −1.620 |
| 7 | $TE_{111}$ | 98920 | 98073 | 97319 | 103151 | 0.856 | 1.618 |
| 8 | $TE_{022}$ | 145950 | 145189 | 146297 | 145618 | 0.521 | −0.238 |
| 9 | $TE_{102}$ | 154285 | 152093 | 153389 | 153550 | 1.421 | 0.581 |
| 10 | $TE_{013}$ | 163295 | 160960 | 162503 | 162648 | 1.430 | 0.485 |

always be higher than Nyquist spatial sampling criterion ($\Delta l < \lambda_{\min}/2$) for the highest expected resonant frequency. Besides that the experience from electromagnetic simulators undermines that a resolution finer than $\lambda_{\min}/7$ is required. However, as depicted in Table 2 even for a relatively coarse discretization with $\Delta l \approx \lambda_{\min}/3$, the agreement in the quality factor values among the analytical, "Leontovich-FEM", "PEC-FEM" as well as the HFSS simulation was better than 4%. Note that HFSS simulation utilizes 350 high-order elements instead of 2733 first-order elements ($\lambda_{\min}/3$). Even though acceptable results are obtained with such a coarse mesh, this is misleading, since the introduction of irregularly shaped objects or slanted scatterers asks for very fine meshes of the order of $\lambda_{\min}/7$ up to $\lambda_{\min}/32$ (as usually observed in electromagnetic simulations) in order to accurately capture their geometry. Recall at this point that eigenanalysis is always very sensitive to the inaccuracies in the description of boundary surfaces (e.g., the well-known stair-case effects in finite different methodologies). Explicitly, the quality factor calculated from the PEC numerical eigenfunctions according to Section 2.2.2 (also depicted in Table 2), solving the electric ($E$-field) wave equation offered an acceptable deviation of less than 1.7% even for a mesh resolution of $\lambda/3$. The substantially lower computational requirements of the "PEC-FEM" formulations led us to utilize them for all the following numerical studies. However, the "Leontovich-FEM" can be adopted whenever the necessary computer resources are available or a more straightforward and convenient approach is desired.

### 4.2. Establishment of Mode Stirrer's Design Guidelines

Inside the reverberation chamber, the mode stirrer is actually the most important object. After the introduction of the mode stirrer two main effects are studied: the resonant frequency and quality factor shift due to the presence of the mode stirrer and the frequency variation during its rotation. As noted in Section 1, the mode stirrer scatters the field aiming at a time averaged homogeneous field-distribution in the testing region. This phenomenon can be explained using eigenanalysis; the eigenvalues (resonant frequencies) are dispersed in a wide frequency band exciting the same mode at different frequencies — for each position of the mode stirrer at a different time instant — causing in this way a physical frequency sweep.

In order to get an insight into possible spectrum holes-gaps a low and mid frequency bands are zoomed. It is shown from the figures given below that the low frequency band exhibits a lot of gaps while there are few in the mid-band and vanish at higher frequencies. These gaps occur as step-abrupt changes in the spectrum. The low frequency gaps are almost impossible to be eliminated, hence there will be a Lower Usable Frequency (LUF) $f_{LUF}$ for the chamber. The gaps at frequencies higher than $f_{LUF}$ should be covered/eliminated by appropriate location and design of a single or multiple stirrers. Herein we focus on the appropriate shape of a single stirrer, since the scope of the work is toward the establishment of the eigenanalysis as a design tool. The lowest usable frequency is computed according

to the definitions given by the IEC [1]: i) the LUF equals three times the cutoff frequency $f_c$ of the fundamental mode of a cavity with the same dimensions; ii) $f_{LUF}$ is defined as the frequency at which $60 \ldots 100$ modes within an ideal cavity of the same size as the reverberation chamber are above the cutoff, and at least $\vartheta N/\vartheta f = 1.5$ modes/MHz are present. The mode density $\vartheta N/\vartheta f$ can be calculated as [6, Page 11]:

$$\frac{\vartheta N}{\vartheta f} = 8\pi abd\frac{f^2}{c^3} - (a+b+d)\frac{1}{c} \tag{28}$$

where $a$, $b$, $d$ are the reverberation chamber's dimensions, $f$ the resonant frequency, and $c$ the speed of light. For the empty cavity-chamber studied above (Table 1) its $LUF_1 = 3.48\,\text{MHz} = 144\,\text{MHz}$ according to the first definition, while it is $LUF_2 = 202\,\text{MHz}$ according to the second definition of Eq. (28). By simulating a set of five different mode stirrers and exploiting their features this procedure aims at the establishment of the proposed design guidelines. The choice of each mode stirrer is not arbitrary, but it is inspired by the Ph.D. thesis of Dr. Bruns [6, Page 101]. The investigation starts with two mode stirrers formed by scatterers parallel and vertical to the horizontal cross-section respectively and continues with a type of slant oriented which is also studied by Bruns [6]. Finally, two mode stirrers are devised comprised of inclined attached scatterers, aiming at the disturbance of all field components.

### *4.2.1. First Mode Stirrer*

The first-mode stirrer is a typical cylindrical metallic stirrer consisting of four metallic paddles, as shown in Figure 4. The cylindrical axle height is $h = 1.0\,\text{m}$ and has a radius of $r = 0.25\,\text{m}$ meters. Each planar scatterer has dimensions $l = 0.85\,\text{m}$ and $w = 0.65\,\text{m}$, while its thickness is $d = 0.05\,\text{m}$. The whole structure is metallic and modeled assuming finite copper conductivity ($\sigma_{Cu} = 58 \cdot 10^6\,\text{S/m}$).

To accurately model the fine details of the mode stirrer and specifically the extremely thin paddles compared with the reverberation chamber's dimensions, a mesh of 292056 tetrahedrals was initialized. Taking into consideration the mesh density, the sampling step can be computed for each mode (150 modes have been totally calculated). Subtracting from the total number of the tetrahedrals that coincide with the metallic surfaces of the structure, since the mesh is adaptively increased in these areas, the number of inner tetrahedrals can be calculated. Using the remaining number of tetrahedrals, the sampling step can be approximately estimated, assuming that the tetrahedrals are normally distributed in the chamber's volume and accepting that a sample (this is actually a cubic element in three dimensions) corresponds to 12 tetrahedrals in the worst case. A more optimistic approach is to assume that 5 tetrahedrals correspond to a cubic sample. In Table 8, the sampling step is tabulated for the first and last modes, respectively. Only the linear PEC formalism was utilized to compute both the resonant frequency and the quality factor of the structure, while the "Leontovich-FEM" was not further used since as it is proved in the empty cavity simulation (Table 2), a mesh 6 times denser is demanded to describe the same problem with the same accuracy, which is of course inefficient.

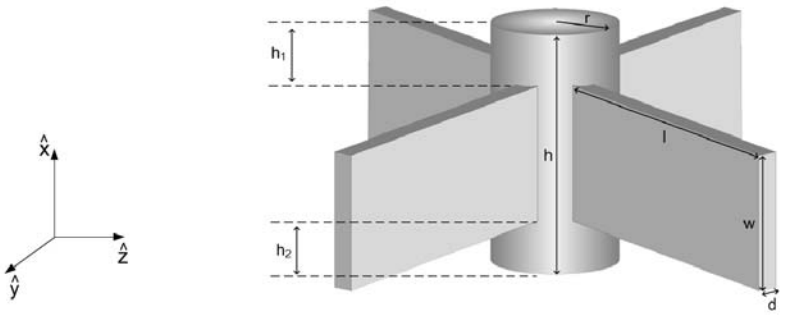


**Figure 4.** Metallic ($\sigma_{Cu} = 58 \cdot 10^6\,\text{S/m}$) mode stirrer #1 with cylindrical axis and four parallelepiped paddles transverse to each other. Typical dimensions are assumed as: $l = 0.85\,\text{m}$, $w = 0.65\,\text{m}$, $d = 0.05\,\text{m}$, $r = 0.25\,\text{m}$, $h = 1.0\,\text{m}$, $h_1 = 0.175\,\text{m}$, $h_2 = 0.175\,\text{m}$.

The introduction of the mode stirrer shifts the resonant frequencies. Table 3 depicts the frequency shift of the first ten resonances with respect to the empty cavity and shows the corresponding quality factor shift. The decrease of the resonant frequencies can also be explained by the example of any ridged waveguide [39]. The introduction of a ridge in a region of maximum electric field decreases the cutoff frequency or the cutoff wavenumber $k_c$ and in turn the resonant frequency, since it is $k_r^2 = \omega_r^2\mu\epsilon = k_c^2+\beta^2$. The decrease of the quality factor (Table 3) was something expected, since the introduction of the finite conductivity metallic scatterers increases the ohmic losses. However, a reduction about 50% corresponding to doubling the losses is not justified by the size of the mode stirrer or its total surface ($\sim$6.85 m$^2$) with respect to the chamber internal surface ($\sim$76 m$^2$), which is only 11.1%. This reduction is in contrary justified by the placement of these scatterers in the area of maximum field intensity for most of the modes. The variation of the frequency during the rotation of the mode stirrer is explored in the Subsection 4.2.

The rotation of the mode stirrer by a 5-degree step yields the first 150 modes spectrum. In Figure 5(a), the variation of the first mode is shown. A 57.3 kHz band coverage is calculated, while for a $Q \cong 69000$ at $f_0 \cong 43$ MHz, its bandwidth is $B_{3\,\mathrm{dB}} = f_0/Q \cong 0.62$ kHz. In Figure 5(b), the stirrer's effect on mode #34 at the $LUF_1$ given from the first definition of IEC ($f = 3f_c$) is shown. A larger frequency sweep of the order of 550 kHz is calculated, while in this case the frequency variation versus stirrer's rotation is faster. This behavior was actually expected, since the mode stirrer is more efficient beyond the lowest usable frequency. In Figure 6(a), the frequency spectrum of the first 150 modes is

**Table 3.** Shift in resonant frequencies and in the quality factor of the reverberation chamber when loaded with the mode stirrer #1 of Figure 4.

| | | frequency MHz | | | quality factor | | |
|---|---|---|---|---|---|---|---|
| | Mode | empty-RC analytical | loaded-RC 292056 el. | Freq. shift % | empty-RC analytical | 292056 el. $E$-field | qual. fact. change % |
| 1 | $TE_{011}$ | 47.8 | 43.4 | −9.21 | 109096 | 69531 | −36.27 |
| 2 | $TE_{012}$ | 69.8 | 54.1 | −22.49 | 137114 | 73786 | −46.19 |
| 3 | $TE_{021}$ | 79.2 | 55.1 | −30.43 | 116487 | 72918 | −37.40 |
| 4 | $TE_{101}$ | 80.7 | 68.9 | −14.62 | 137870 | 73395 | −46.76 |
| 5 | $TM_{110}$ | 83.5 | 71.2 | −14.73 | 125939 | 67237 | −46.61 |
| 6 | $TM_{111}$ | 88.3 | 80.9 | −8.32 | 109821 | 78739 | −28.30 |
| 7 | $TE_{111}$ | 89.6 | 85.2 | −4.91 | 98920 | 33183 | −66.45 |
| 8 | $TE_{022}$ | 93.7 | 92.2 | −1.60 | 145950 | 101501 | −30.45 |
| 9 | $TE_{102}$ | 94.2 | 93.4 | −0.85 | 154285 | 91576 | −40.64 |
| 10 | $TE_{013}$ | 96.0 | 94.0 | −33.33 | 163295 | 59322 | −63.67 |

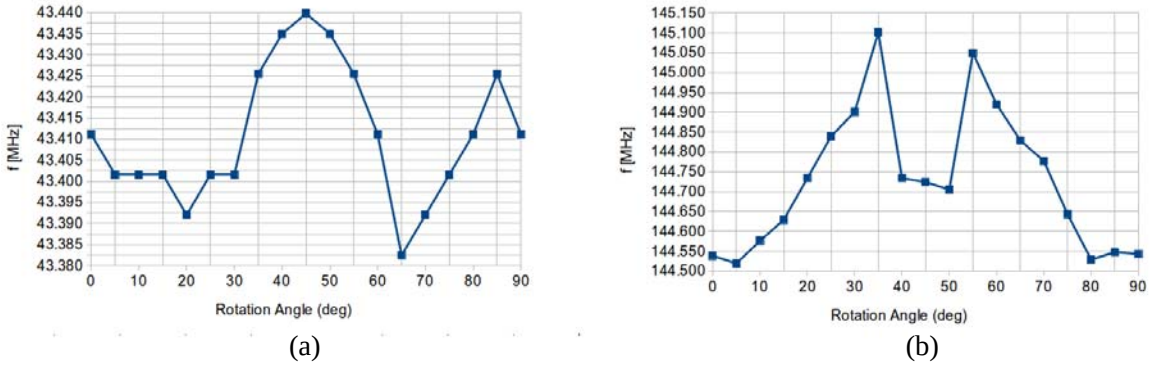


**Figure 5.** Mode variation during the mode stirrer #1 rotation: (a) variation of the 1st resonant mode and (b) variation of the mode #34 estimated at the $LUF_1$ ($f = 3f_c$).

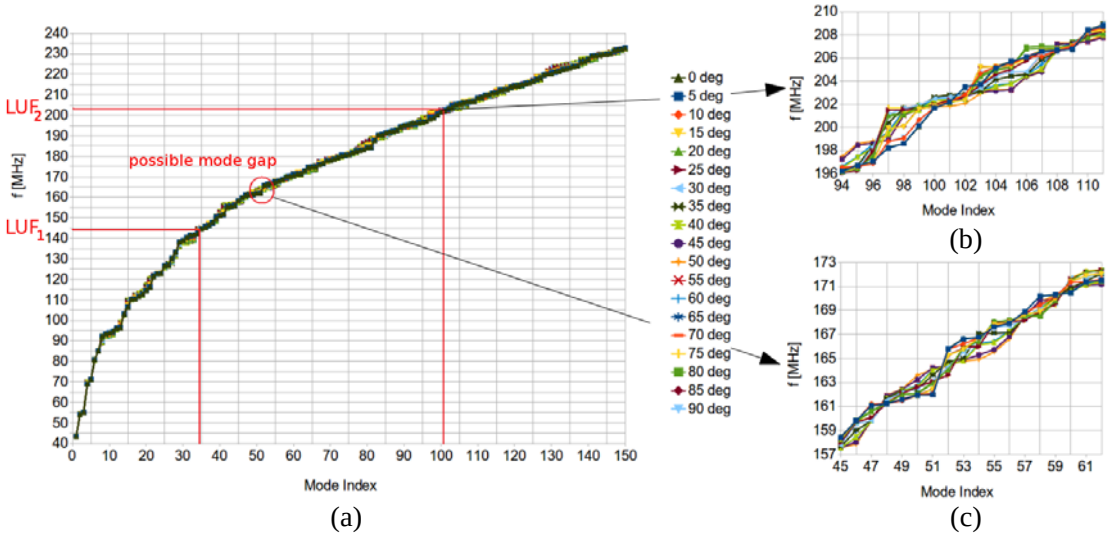


**Figure 6.** Frequency spectrum during the rotation of the mode stirrer #1 of Figure 4: (a) frequency spectrum of the first 150 modes, (b) zoom around $LUF_2$ where $\vartheta N/\vartheta f = 1.5$ modes/MHz, and (c) zoom at an observed mode gap.

shown. The purpose of Figure 6 and the corresponding figure for each mode stirrer is to observe whether the frequency spectrum and particularly close to LUF is continuously covered and more importantly to reveal any spectrum holes-gaps which are catastrophic for measurements accuracy. Recall that the resonant frequencies are discrete, but they are shifted as the mode stirrer is rotated. The question is how efficiently the mode stirrer shifts the resonant frequency in order to provide a "continuous" frequency coverage with gaps smaller than the modes bandwidth. Figure 6 shows that below $LUF_1 = 144$ MHz there are so many possible gaps-holes that this band is useless. However, for this #1 stirrer gaps continue to exist above $LUF_1$ at 152 and 164 MHz and up to $LUF_2 = 202$ MHz. Two of these suspicious areas are then zoomed in Figures 6(b), 6(c) where it is observed that there are not any obvious gaps but very low mode density at 164 or 200 MHz (only one or two modes). As shown in Table 3, the mode 3-dB bandwidth is about 1 kHz, thus there are indeed frequencies with poor mode density (gaps indeed) which may yield unacceptable measurement accuracy. These problematic sub-bands ("gaps") could be filled with modes by a more appropriate stirrer design. Besides these observations, Figure 6 shows that above $LUF_2$ a high mode density is achieved.

One point that should be noted is that both the symmetry of the reverberation chamber and the mode stirrer permit the simulation for only a rotation of 90 degrees. This is too important since time and computational cost are saved. Each simulation demands 55.6 minutes from the initialization of an almost 290000 tetrahedrals mesh up to the complete eigenvalues spectrum computation. For each eigenvalue and the corresponding eigenvector computation, 5 seconds are demanded. The modes stirrer of Figure 4 affects the $E_x$ component when it is introduced; however, during its rotation its blades change their relative orientation from (parallel to $E_y$, normal to $E_z$) to vice versa, hence the variation in $E_y$, $E_z$ distribution is higher. The next trial refers to scatterers parallel to $yz$ horizontal base plane.

### *4.2.2. Second Mode Stirrer*

The second mode stirrer shown in Figure 7 consists again of a cylindrical axle of height $h = 1.0$ m and radius $r = 0.25$ m, and two square paddles of length $l = 1.2$ m and thickness $d = 0.02$ m. To accurately model the fine details of the mode stirrer, a mesh of 290227 tetrahedrals was initialized. The introduction of the mode stirrer lowers both the resonant frequencies and the quality factor as shown in Table 4. Comparing Tables 4 and 3 it is observed that mode stirrer #2 produces similar frequency shift to #1 for the first mode but much less for the higher order modes. Also the quality factor of $TM_{111}$ and $TE_{111}$ modes, remains almost unaffected, especially for the higher modes, with respect to the empty cavity. This can be justified by a minimum of the tangential magnetic field over the scatterers.

**Table 4.** Reverberation chamber's resonant frequencies and quality factor, loaded with the mode stirrer #2 of Figure 7.

| | | frequency MHz | | | quality factor | | |
|---|---|---|---|---|---|---|---|
| | Mode | empty-RC analytical | loaded-RC 290227 el. | Freq. shift % | empty-RC analytical | 290227 el. *E*-field | qual. fact. change % |
| 1 | $TE_{011}$ | 47.8 | 39.08 | −18.24 | 109096 | 74050 | −32.12 |
| 2 | $TE_{012}$ | 69.8 | 67.85 | −2.79 | 137114 | 92819 | −32.31 |
| 3 | $TE_{021}$ | 79.2 | 69.58 | −12.15 | 116487 | 95165 | −18.30 |
| 4 | $TE_{101}$ | 80.7 | 71.61 | −11.26 | 137870 | 107807 | −21.81 |
| 5 | $TM_{110}$ | 83.5 | 71.97 | −13.81 | 125939 | 55376 | −56.03 |
| 6 | $TM_{111}$ | 88.3 | 81.78 | −7.38 | 109821 | 106473 | −3.05 |
| 7 | $TE_{111}$ | 89.6 | 87.69 | −2.13 | 98920 | 102762 | 3.88 |
| 8 | $TE_{022}$ | 93.7 | 88.12 | −5.96 | 145950 | 106381 | −27.11 |
| 9 | $TE_{102}$ | 94.2 | 94.05 | −0.16 | 154285 | 94645 | −38.66 |
| 10 | $TE_{013}$ | 96.0 | 95.95 | −0.05 | 163295 | 137325 | −15.90 |

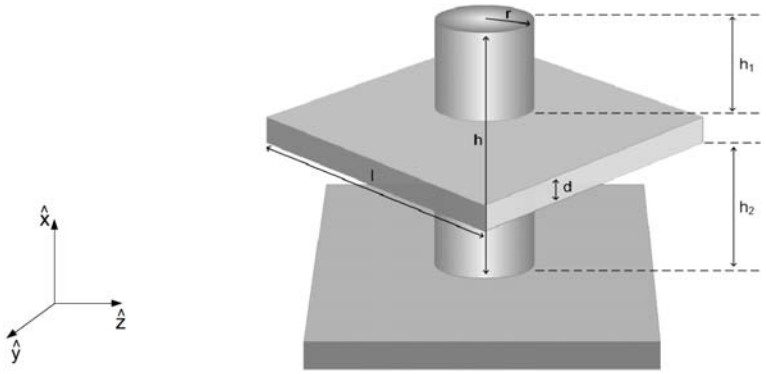


**Figure 7.** Mode stirrer #2 with a cylindrical axis and two (2) square scatterers rotated by an angle of 45° degrees to each other. The mode stirrer is totally metallic with copper conductivity $\sigma_{Cu} = 58 \cdot 10^6\,\mathrm{S/m}$. Its dimensions are: $l = 1.2\,\mathrm{m}$, $d = 0.02\,\mathrm{m}$, $r = 0.25\,\mathrm{m}$, $h = 1.0\,\mathrm{m}$, $h_1 = 0.32\,\mathrm{m}$, $h_2 = 0.64\,\mathrm{m}$ [6].

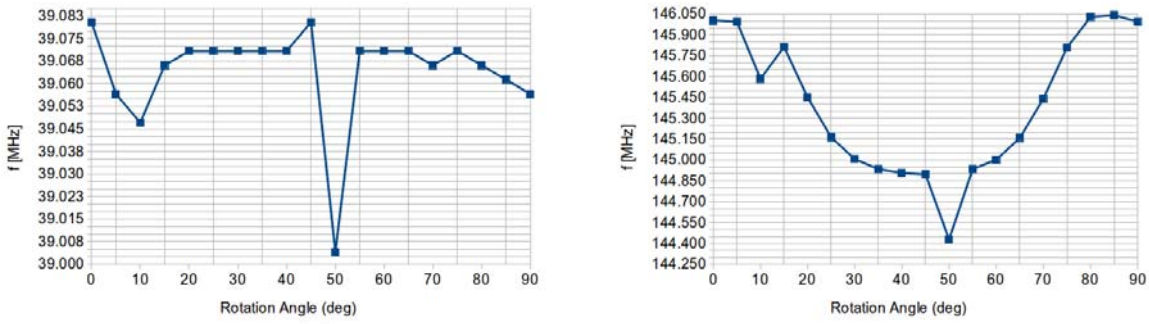


**Figure 8.** Mode variation during the mode stirrer #2 rotation: (a) variation of the 1st resonant mode and (b) variation of the mode #37 estimated at the $LUF_1$ ($f = 3f_c$).

The rotation of the mode stirrer by a 5 degree step yields the first 150-mode spectrum. In Figure 8(a), the variation of the first mode is shown, where a 80 kHz band coverage can be calculated. Reasonable frequency stirring occurs only within two small angular sectors around 10° and 50°. In Figure 8(b), the mode #37 at $LUF_1$ is shown, where a coverage of 1.61 MHz occurs during the stirrer's

rotation. Efficient mode stirring occurs over the whole angular sector for this high order mode. In Figure 9(a), the frequency spectrum of the first 150 modes is shown. A mode gap occurs above $LUF_1 = 144\,\text{MHz}$ which is around 170 MHz and has been chosen for a detailed study. The frequency jump is now more clear in Figure 9(c) compared with the corresponding gap of Figure 9(c). Moreover, in Figure 9(b) the efficiency of the stirrer at and above $LUF_2 = 202\,\text{MHz}$ can be clearly observed, since the whole area is covered by the excited modes. Figure 9(c) shows a clear gap in the modes spectrum at 174 MHz. Besides that, Figures 6 and 9 depict a lot of small steps in the frequency spectrum between $LUF_1$ and $LUF_2$, which present at least low mode density.

### *4.2.3. Third Mode Stirrer*

The third mode stirrer consists of the same cylindrical body ($h = 1.0\,\text{m}$ height, $r = 0.25\,\text{m}$ radius), but with three quite different scatterers hinged from this body with an angle of 25° degrees between each other as shown in Figure 10. The slanted scatterers of the stirrer form the letter Z, thus this kind of mode stirrer is usually called Z-type [6]. The scatterers at the top and bottom of the cylinder have a

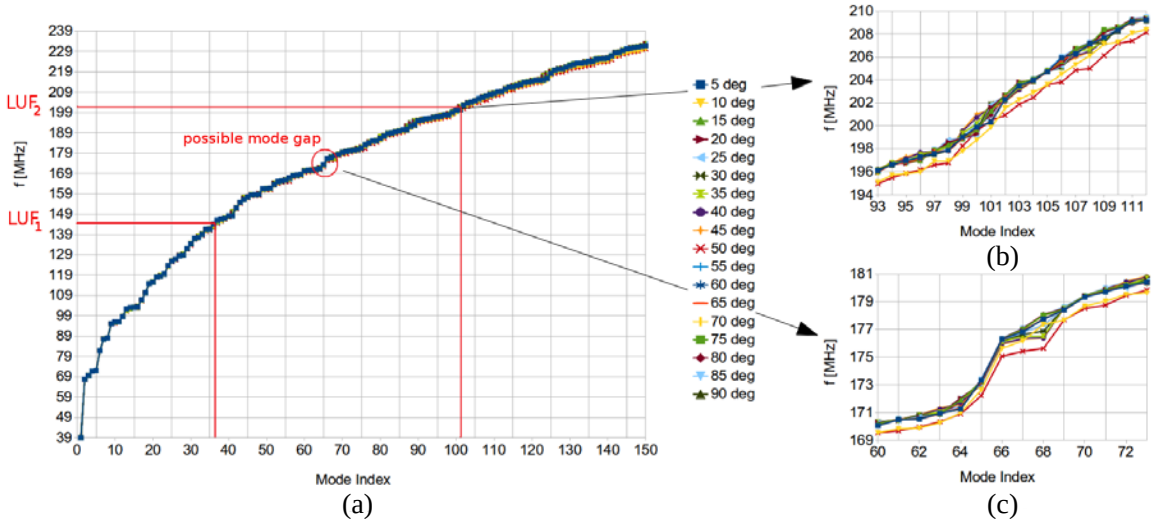


**Figure 9.** Frequency spectrum during the rotation of the mode stirrer #2 of Figure 7: (a) frequency spectrum of the first 150 modes, (b) zoom around $LUF_2$ where $\vartheta N/\vartheta f = 1.5$ modes/MHz, and (c) zoom around an observed mode gap.

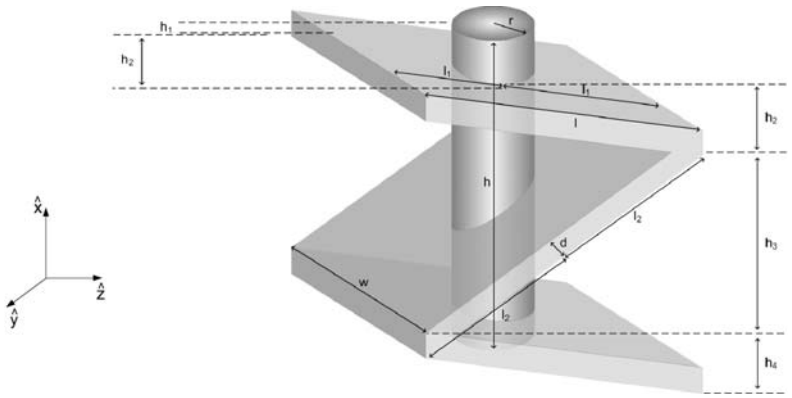


**Figure 10.** Z metallic mode stirrer #3, [6] of copper conductivity $\sigma_{Cu} = 58 \cdot 10^6\,\text{S/m}$. Its dimensions are: $l = 2.0\,\text{m}$, $w = 0.6\,\text{m}$, $d = 0.01\,\text{m}$, $r = 0.25\,\text{m}$, $l_1 = l/2$, $l_2 = l$, $h = 1.0\,\text{m}$, $h_1 = 0.1\,\text{m}$, $h_2 = 0.17\,\text{m}$, $h_3 = 0.35\,\text{m}$, $h_4 = 0.34\,\text{m}$.

surface of $2.0 \times 0.6\,\mathrm{m}^2$ and thickness of 0.01 m, while the middle scatterer has a surface of $3.0 \times 0.6\,\mathrm{m}^2$. The structure is totally metallic with copper conductivity $\sigma_{Cu} = 58 \cdot 10^6\,\mathrm{S/m}$. To accurately model the fine details of the mode stirrer, a mesh of 305150 tetrahedrals was initialized. The frequency and quality factor shift are shown in Table 5. Compared to the first stirrer (Table 3), it presents similar behavior to a more homogeneous shift caused in the higher order modes. The presence of the slanted scatterers disturbs all the field components, and this is depicted by the smoother resonant frequency variation in Table 5 than Tables 3 and 4.

In Figure 11(a), the variation of the first mode is shown, where a 2.0 MHz band coverage is calculated, but the stirring is completely ineffective in the angular sector from 50° to 90°. In Figure 11(b), the mode #35 at the $LUF_1$ is shown, where its band coverage decreases to 1.11 MHz, but the frequency stirring is efficient over the whole angular sector. Although there is a clear mode hole-gap at 168 MHz (Figure 12(c)), stirrer #3 appears more efficient than #2 and #1, since its mode spectrum in Figure 12 is more continuous, with smaller steps (possible low mode density) than those in Figures 9 and 6. This observation is clearly valid in the band between $LUF_1$ and $LUF_2$, while stirrer #3 has a more homogeneous mode spectrum even below $LUF_1$. Note that above $LUF_2$ all stirrers behave quite well with homogeneous mode density.

An overview of the previous investigations reveals that:

**Table 5.** Reverberation chamber's resonant frequencies and quality factor, loaded with the mode stirrer #3 of Figure 10.

| | | frequency MHz | | | quality factor | | |
|---|---|---|---|---|---|---|---|
| | Mode | empty-RC analytical | loaded-RC 305150 el. | Freq. shift % | empty-RC analytical | 305150 el. $E$-field | qual. fact. change % |
| 1 | $TE_{011}$ | 47.8 | 37.91 | −20.69 | 109096 | 77874 | −28.62 |
| 2 | $TE_{012}$ | 69.8 | 55.48 | −20.52 | 137114 | 84682 | −38.24 |
| 3 | $TE_{021}$ | 79.2 | 71.17 | −10.14 | 116487 | 65484 | −43.78 |
| 4 | $TE_{101}$ | 80.7 | 71.75 | −11.09 | 137870 | 106798 | −22.54 |
| 5 | $TM_{110}$ | 83.5 | 71.76 | −14.06 | 125939 | 66160 | −47.47 |
| 6 | $TM_{111}$ | 88.3 | 78.92 | −10.62 | 109821 | 116559 | 6.14 |
| 7 | $TE_{111}$ | 89.6 | 82.76 | −7.63 | 98920 | 102040 | 3.15 |
| 8 | $TE_{022}$ | 93.7 | 86.96 | −7.19 | 145950 | 100978 | −30.81 |
| 9 | $TE_{102}$ | 94.2 | 89.39 | −5.11 | 154285 | 98996 | −35.84 |
| 10 | $TE_{013}$ | 96.0 | 95.01 | −1.03 | 163295 | 103557 | −36.58 |

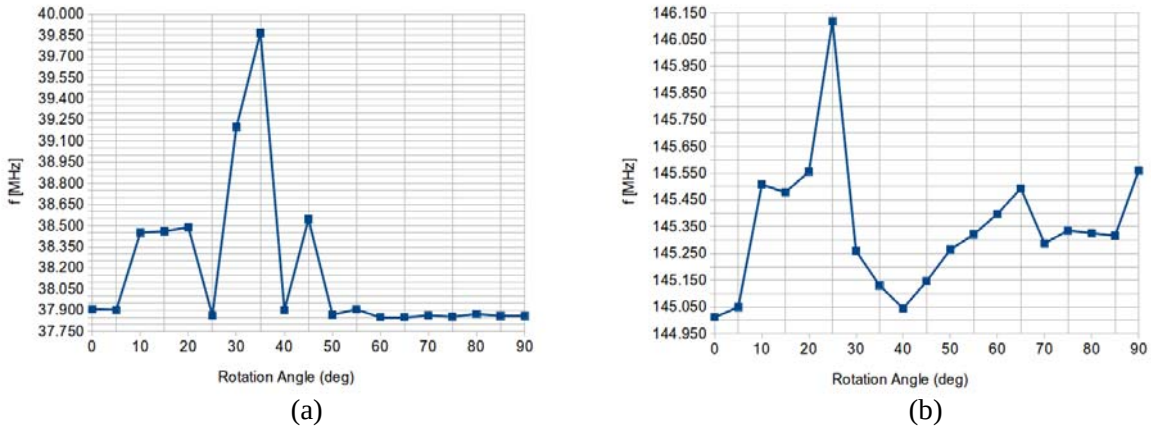


**Figure 11.** Mode variation during the mode stirrer #3 rotation: (a) variation of the 1st resonant mode and (b) variation of the mode #35 estimated at the $LUF_1$ ($f = 3f_c$).

i The horizontal plane scatterers (Figure 7) cause a severe reduction in the resonant frequencies of modes 1st to 8th (Table 4), mainly perturbing simultaneously the horizontal components.

ii The vertical plane scatterers of Figure 4 perturb $E_y$, $E_z$ but at different locations and cause reduction on the first three $TE$ modes and $TM_{111}$ (Table 3). What is important is that this stirrer retains the chamber's full height at angles between the scatterers, thus efficiently covering the low frequency spectrum.

iii The slanted scatterers of Figure 10 disturb all electric field components (including the vertical $E_x$), but their projections are overlapping and exclude any field access to full height.

The question is then how to combine the three types of scatterers, avoiding their projection overlapping,

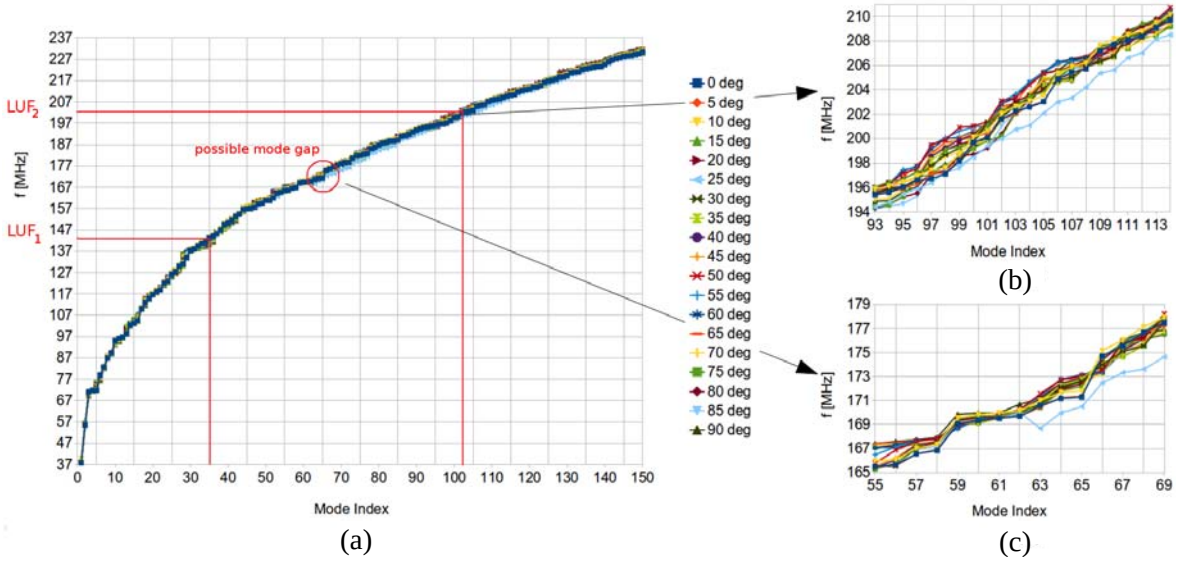


**Figure 12.** Frequency spectrum during the rotation of the mode stirrer #3 of Figure 10: (a) frequency spectrum of the first 150 modes, (b) zoom around $LUF_2$ where $\vartheta N/\vartheta f = 1.5$ modes/MHz, and (c) zoom around an observed mode gap.

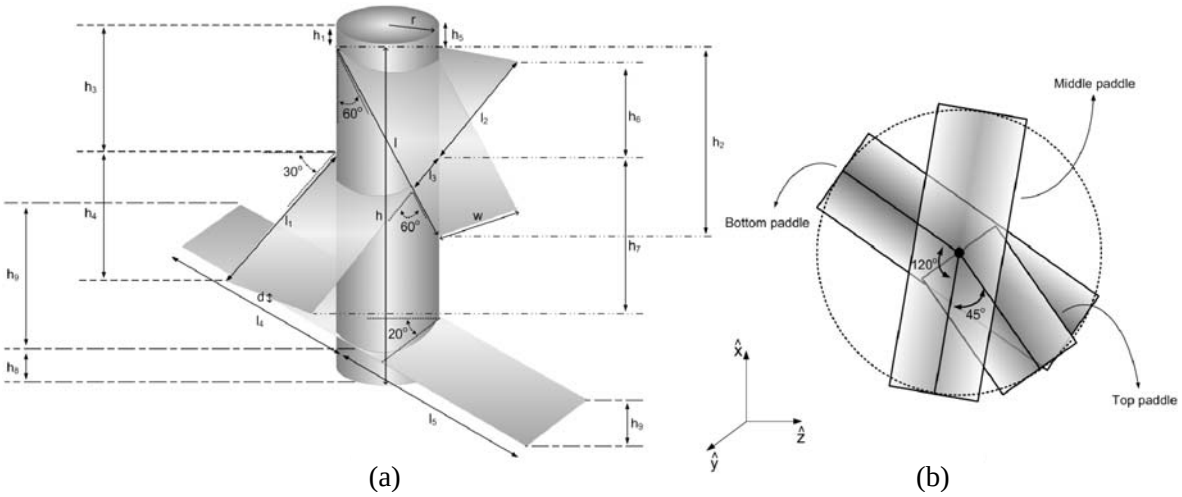


**Figure 13.** (a) Mode stirrer #4 with a cylindrical axis and three arbitrarily hinged scatterers. The mode stirrer is totally metallic with copper conductivity $\sigma_{Cu} = 58 \cdot 10^6$ S/m. Its dimensions are: $l = 1.0$ m, $w = 0.8$ m, $d = 0.01$ m, $r = 0.25$ m, $h = 1.0$ m, $h_1 = 0.1$ m, $h_2 = 0.5$ m, $h_3 = 0.3$ m, $h_4 = 0.5$ m, $h_5 = 0.14$ m, $h_6 = 0.21$ m, $h_7 = 0.79$ m, $h_8 = 0.1$ m, $h_9 = 0.3$ m, $l_1 = 1.0$ m, $l_2 = 0.42$ m, $l_3 = 0.58$ m, $l_4 = 1.0$ m, $l_5 = 1.0$ m. (b) Plan view of the mode stirrer.

which is answered by the next 4th-mode stirrer (first proposed herein) which also slants some of them side wards, besides slanting the scatterers downwards. Also, as noted in the guidelines (Section 3) it retains scatterers at different heights, as shown in Figure 13.

### *4.2.4. Fourth Mode Stirrer*

For the fourth-mode stirrer, a cylindrical axis is introduced with height $h = 1.0\,\text{m}$ and radius $r = 0.25\,\text{m}$, as the main body, where three paddles of arbitrary angle are hinged over as shown in Figure 13(a). Each paddle is $d = 0.01\,\text{m}$ thick and has a surface of $0.8 \times 1.0\,\text{m}^2$, while the whole structure is metallic and made of copper. To check if there is any overlap between the paddles, a plan view of their projection is given in Figure 13(b). As shown, there is a large non-overlapping angular sector which permits the resonance of the lower modes. To accurately model the fine details of the mode stirrer, a mesh of 335250 tetrahedrals was initialized. The resonant frequency and quality factor shift are tabulated in Table 6. Comparing the two last mode stirrers, one observes that going from #3 to #4 the quality factor reduction becomes more uniform while resonant frequency shift is increased and becomes more uniform up to the 8th mode. In Figure 14(a), the variation of the first mode is shown, where a 40 kHz band coverage is calculated, but it is important to observe that this novel #4 stirrer efficiently varies the frequency over the whole angular sector even for the first mode (just compare Figure 14(a) with Figures 11(a), 8(a) and 5(a)). In Figure 14(b), the mode #37 at the $LUF_1$ ($f = 3f_c$) is shown, where the band coverage is 2.26 MHz. Figure 15 reveals that this novel #4 stirrer performs efficiently starting from $LUF_1 = 44\,\text{MHz}$ and above, without any gaps in the band from $LUF_1$ to $LUF_2$. Furthermore, besides a

**Table 6.** Reverberation chamber's resonant frequencies and quality factor, loaded with the mode stirrer #4 of Figure 13.

| | | frequency MHz | | | quality factor | | |
|---|---|---|---|---|---|---|---|
| | Mode | empty-RC analytical | loaded-RC 335250 el. | Freq. shift % | empty-RC analytical | 335250 el. *E*-field | qual. fact. change % |
| 1 | $TE_{011}$ | 47.8 | 41.00 | −14.23 | 109096 | 82549 | −24.33 |
| 2 | $TE_{012}$ | 69.8 | 55.98 | −19.80 | 137114 | 78243 | −42.94 |
| 3 | $TE_{021}$ | 79.2 | 63.59 | −20.01 | 116487 | 76883 | −34.00 |
| 4 | $TE_{101}$ | 80.7 | 71.53 | −11.36 | 137870 | 105161 | −23.72 |
| 5 | $TM_{110}$ | 83.5 | 72.11 | −13.64 | 125939 | 58350 | −53.67 |
| 6 | $TM_{111}$ | 88.3 | 80.44 | −8.90 | 109821 | 76093 | −30.71 |
| 7 | $TE_{111}$ | 89.6 | 81.92 | −8.57 | 98920 | 95121 | −3.84 |
| 8 | $TE_{022}$ | 93.7 | 87.04 | −7.11 | 145950 | 86350 | −40.84 |
| 9 | $TE_{102}$ | 94.2 | 88.61 | −5.93 | 154285 | 102660 | −33.46 |
| 10 | $TE_{013}$ | 96.0 | 90.91 | −5.30 | 163295 | 97909 | −40.04 |

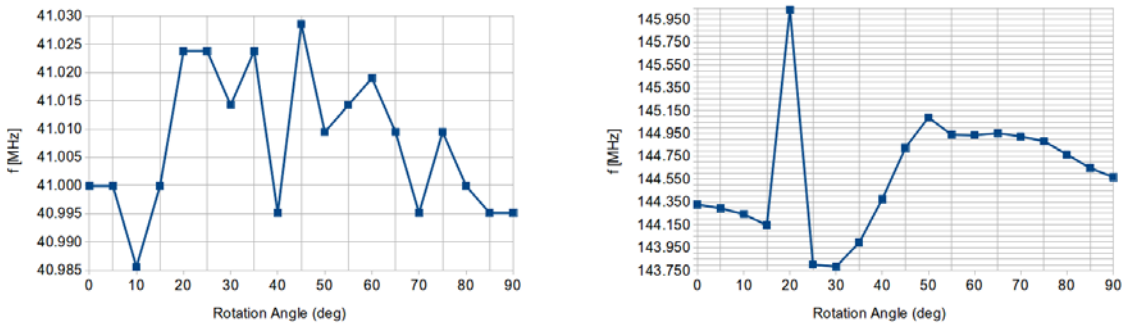


(a) (b)

**Figure 14.** Mode variation during the mode stirrer #1 rotation: (a) variation of the 1st resonant mode and (b) variation of the mode #34 estimated at the $LUF_1$ ($f = 3f_c$).

clear mode gap at 130 MHz, it also provides efficient frequency stirring down to 90 MHz ($\approx 2f_c$). Hence, it is clearly superior to stirrers #1, 2, 3.

### *4.2.5. Fifth Mode Stirrer*

For the final mode stirrer, an evolution of the last one is introduced. As shown in Figure 16(a), this kind of mode stirrer has three more paddles than the previous one. This careful placement of the scatterers disturbs the field in any direction and for any angle, producing the desirable field homogeneity. The geometrical features of these additional scatterers are the same as that for the fourth-mode stirrer (Figure 13(a)). To check if there is any overlap between the paddles, a projections plan view is given in Figure 16(b). It is then verified that there is a large non-overlapping angular sector offering field access

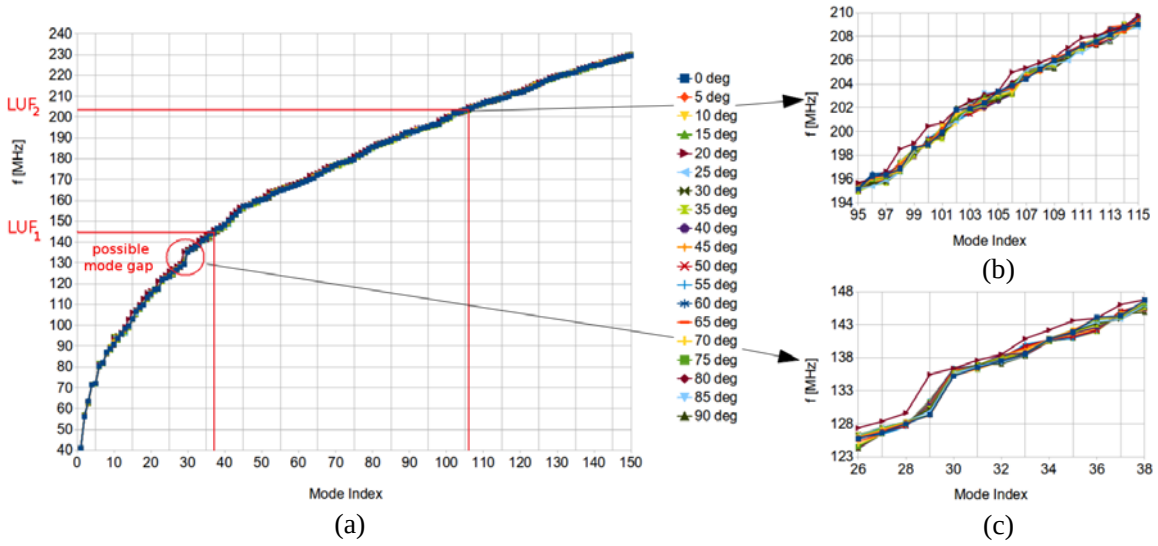


**Figure 15.** Frequency spectrum during the rotation of the mode stirrer #4 of Figure 13: (a) frequency spectrum of the first 150 modes, (b) zoom around $LUF_2$ where $\vartheta N/\vartheta f = 1.5$ modes/MHz, and (c) zoom around an observed mode gap.

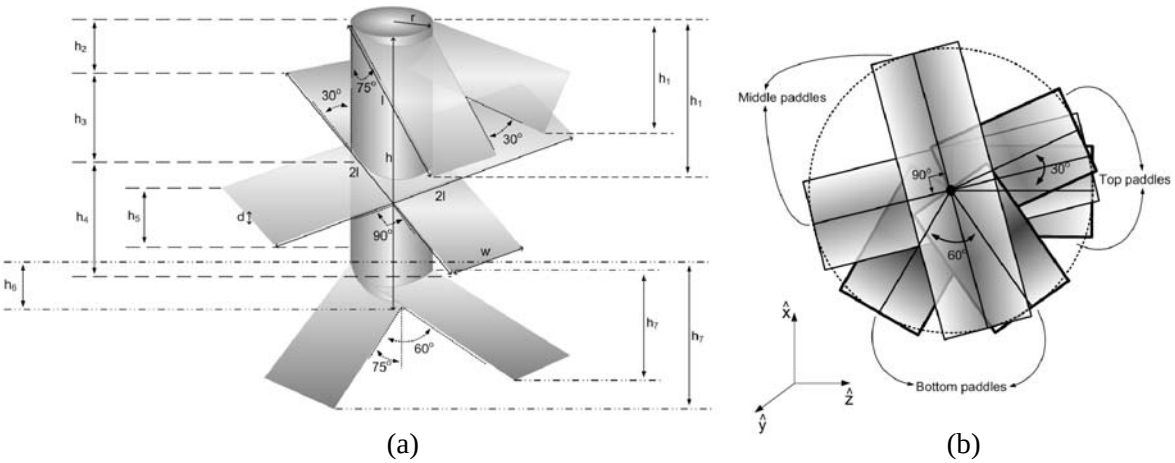


**Figure 16.** (a) Mode stirrer #5 with a cylindrical axis and six arbitrarily hinged scatterers. The mode stirrer is totally metallic with copper conductivity $\sigma_{Cu} = 58 \cdot 10^6$ S/m. Its dimensions are: $l = 1.0$ m, $w = 0.8$ m, $d = 0.01$ m, $r = 0.25$ m, $h = 1.0$ m, $h_1 = 0.26$ m, $h_2 = 0.14$ m, $h_3 = 0.21$ m, $h_4 = 0.5$ m, $h_5 = 0.2$ m, $h_6 = 0.15$ m, $h_7 = 0.26$ m. (b) Plan view of the mode stirrer.

**Table 7.** Reverberation chamber's resonant frequencies and quality factor, loaded with the mode stirrer #5 of Figure 16.

| | | frequency MHz | | | quality factor | | |
|---|---|---|---|---|---|---|---|
| | Mode | empty-RC analytical | loaded-RC 690825 el. | Freq. shift % | empty-RC analytical | 690825 el. $E$-field | qual. fact. change % |
| 1 | $TE_{011}$ | 47.8 | 39.39 | −17.59 | 109096 | 69532 | −36.27 |
| 2 | $TE_{012}$ | 69.8 | 58.76 | −15.82 | 137114 | 73786 | −46.19 |
| 3 | $TE_{021}$ | 79.2 | 59.80 | −24.49 | 116487 | 72918 | −37.40 |
| 4 | $TE_{101}$ | 80.7 | 71.01 | −12.01 | 137870 | 73395 | −46.77 |
| 5 | $TM_{110}$ | 83.5 | 72.08 | −13.68 | 125939 | 67237 | −46.61 |
| 6 | $TM_{111}$ | 88.3 | 78.61 | −10.97 | 109821 | 33183 | −69.78 |
| 7 | $TE_{111}$ | 89.6 | 79.73 | −11.02 | 98920 | 78740 | −20.40 |
| 8 | $TE_{022}$ | 93.7 | 81.89 | −12.60 | 145950 | 101501 | −30.45 |
| 9 | $TE_{102}$ | 94.2 | 89.61 | −4.87 | 154285 | 91576 | −40.64 |
| 10 | $TE_{013}$ | 96.0 | 90.90 | −5.31 | 163295 | 59322 | −63.67 |

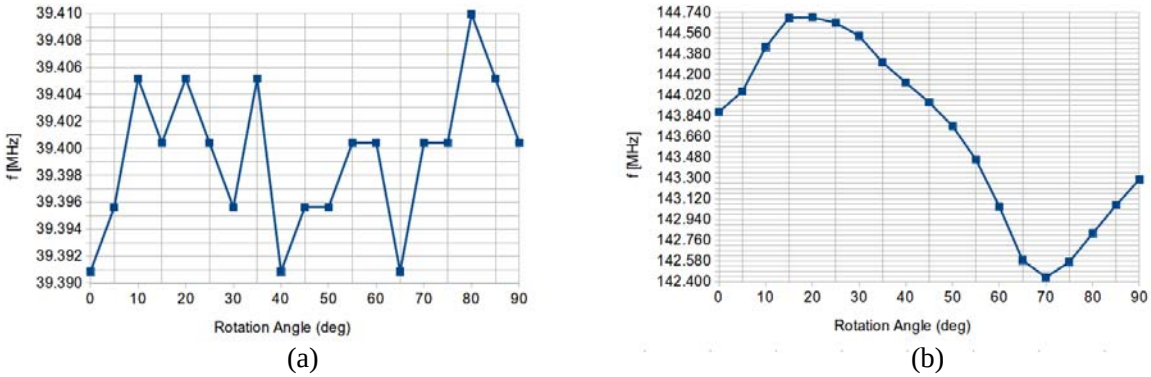


**Figure 17.** Mode variation during the mode stirrer #5 rotation: (a) variation of the 1st resonant mode and (b) variation of the #38 mode estimated at the $LUF_1$ ($f = 3f_c$).

to full height, which permits the resonance of the lower modes. To accurately model the fine details of the mode stirrer, a mesh of 690825 tetrahedrals was initialized. Table 7 shows both the frequency and the quality factor shift.

Figure 17(a) as compared to Figure 14(a) shows that #5 stirrer offers equally fast first-mode frequency variation as #4 but more evenly distributed, or #5 stirrer is equally efficient at all rotation angles. Similarly, #5 offers more homogeneous variations for higher order modes as observed comparing Figure 17(b) with 14(b) at $LUF_2$. The mode spectrum of Figure 18 shows that #5 stirrer can also efficiently stir frequencies from 90 MHz ($\approx 2f_c$) and above as #4 stirrer. Again there is a mode gap, but it is moved higher than $LUF_1 = 144$ MHz and occurs around 152 MHz. It is thus observed that the newly proposed stirrers #4 and #5 can operate even below the lowest frequency ($LUF_1 = 3f_c$) down to a frequency about $2f_c$, but their only drawback is a spectrum hole around $LUF_1$. This gap can be eliminated either by further elaborating on the stirrer design or even by incorporating a second stirrer into the chamber specifically designed to operate around this mode-gap.

### *4.2.6. Mode Stirrers Comparison*

The simulation of each mode stirrer type proves its importance in this structure. Its shape has a significant role, since the simulations show how the field and especially the resonant frequencies vary as the stirrer is rotated. Comparing the stirrers, it can be proved that the two stirrers #4 and #5 proposed herein are the most effective according to the features analyzed in Section 3.

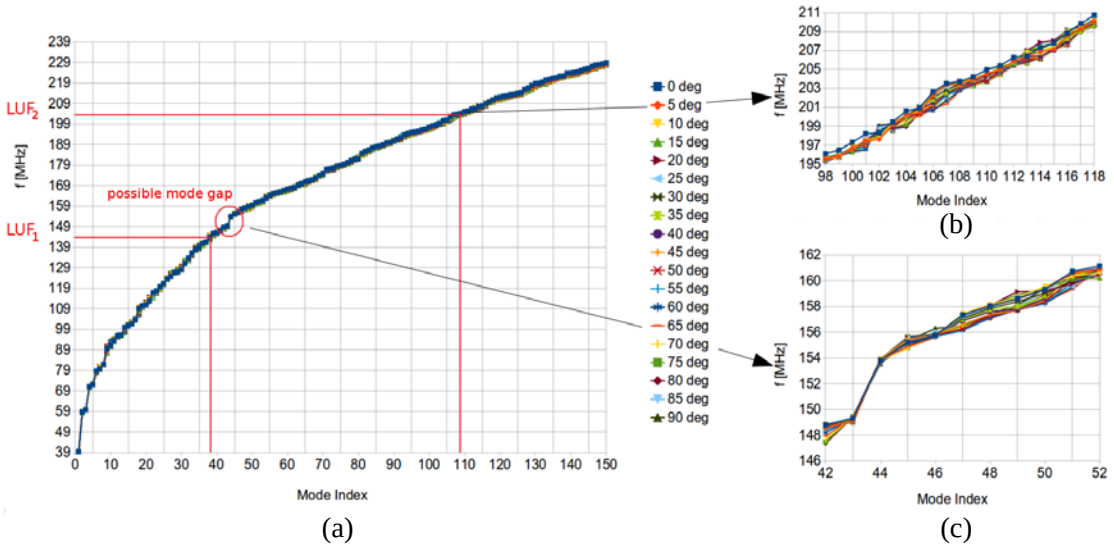


**Figure 18.** Frequency spectrum during the rotation of the mode stirrer #5 of Figure 16: (a) frequency spectrum of the first 150 modes, (b) zoom around $LUF_2$ where $\vartheta N/\vartheta f = 1.5$ modes/MHz, and (c) zoom around an observed mode gap.

**Table 8.** Aggregate table of the proposed mode stirrers, with the results referring to the first 150 modes, simulated using the PEC eigenanalysis tool.

| Feature | 1st mode stirrer Figure 4 | 2nd mode stirrer Figure 7 | 3rd mode stirrer Figure 10 | 4th mode stirrer Figure 13 | 5th mode stirrer Figure 16 |
|---|---|---|---|---|---|
| symmetry | along its axis 90° | along its axis 45° | along its axis 180° | none | none |
| $f_{max}$ 150th mode | 232.62 MHz | 231.83 MHz | 230.40 MHz | 229.36 MHz | 228.77 MHz |
| $f_{min}$ 1st mode | 43.41 MHz | 39.08 MHz | 37.91 MHz | 41.00 MHz | 39.39 MHz |
| BW $f_{max}$-$f_{min}$ | 189.21 MHz | 192.75 MHz | 192.49 MHz | 188.36 MHz | 189.38 MHz |
| BW of the 1st mode | 60 kHz 43.44–43.38 MHz | 80 kHz 39.08–39.00 MHz | 2020 kHz 39.87–37.85 MHz | 70 kHz 41.03–40.96 MHz | 20 kHz 39.41–39.39 MHz |
| number of tetrahedrals | 292056 | 290227 | 305150 | 335250 | 690825 |
| 1st mode sampling step | $\lambda/21$ | $\lambda/22$ | $\lambda/23$ | $\lambda/23$ | $\lambda/29$ |
| 150th mode sampling step | $\lambda/12$ | $\lambda/12$ | $\lambda/12$ | $\lambda/13$ | $\lambda/26$ |
| simulation time | 15.85 min | 15.87 min | 14.96 min | 15.00 min | 105.55 min |
| number of edges (degrees of freedom) | 314016 | 312922 | 300533 | 335516 | 748876 |

In Table 8, an aggregation of the most important characteristics of all the stirrers is tabulated. So, the first one (Figure 4) has four scatterers perpendicular to each other and parallel to the main body, disturbing the field only in $xy$ and $xz$ planes. The second one (Figure 7) consists of the same cylindrical body and two scatterers imposed parallel to the $yz$ plane with an angle of 45° degrees to each other, changing the field in $yz$ plane. An evolution of this one is the third type (Figure 10), z-shaped mode stirrer, which has the same body, but it consists of three scatterers hinged with an angle of 25° degrees to each other along the $yz$ plane. In this way, it achieves a variation in the supplementary planes. The fourth-mode stirrer (Figure 13) combines scatterers from all three previous mode stirrers to yield a field variation in any direction since the scatterers are arbitrarily hinged to its main body. Adding three more scatterers the fifth-mode stirrer (Figure 16) is produced, introducing even more uniform disturbance in the test region almost uniformly perturbing all modes.

#### *4.2.7. Guidelines Verification*

Studying all the stirrers together and comparing their corresponding diagrams of frequency spectrum variation along the stirrer's rotation some very interesting results are deduced. All five studied mode stirrers perform well above the second lowest usable frequency ($LUF_2 = 202\,\text{MHz}$) defined by IEC as in Eq. (28). The Z-type stirrer mostly used in measurements offers more homogeneous mode spectrum than #1 and #2. Inspired from Z-type stirrer and also combining some of the best features for stirrers #1 and #2, two novel stirrers are constructed herein which indeed provide uniform mode density down to $2f_c$ (lower than the $3f_c$ defined by IEC). Their only drawback is a single spectrum gap which requires further elaboration to fill it.

It is important to note here that in general at higher operating frequencies and when reverberation chambers are well stirred, there are indications that losses are increased. Hence, there can be loss of modes orthogonality, and thus modes can be correlated and start exchanging energy. In that case, modal expansion techniques are not rigorously justified, thus modal analysis should be carefully adopted for high frequencies. On the contrary, at low operating frequencies, the modes correlation is highly unlikely to occur. Simultaneously problems of continuous modal coverage exist mainly at the low operating frequency regime, and this is actually consistently addressed within this work.

## 5. CONCLUSION

A finite element eigenanalysis technique including both finite conductivity and dielectric material losses is formulated and tested in the study of electrically large closed cavities. The straightforward FEM formulation where conductivity losses are accounted by directly incorporating the Leontovich boundary condition is proved computationally inefficient requiring parallel processing or computer clusters. In contrast, the novel formulation established herein where the eigenfunctions are acquired from a PEC eigenanalysis, and Leontovich boundary condition is exploited in a post processing procedure and is proved robust and efficient utilizing even personal computers. A set of mode stirrer design guidelines are setup based on the empty cavity electric field eigenfunctions. These are verified through the eigenanalysis of an increasing complexity of the series of mode stirrers, and three are already used in practice and two novel stirrers proposed herein. This process revealed a drawback of the most complex #4 mode stirrer which was overcome by introducing three additional scatterers in accordance with the proposed guidelines. In order for the proposed eigenanalysis to become an efficient design tool for electrically large structures, it is necessary to invent some technique to speed up the solution process, mainly through the reduction of the number of unknowns. Toward this direction we are currently working to adapt a domain decomposition approach to eigenanalysis FEM formulation. Regarding the reverberation chamber and particularly the mode stirrer design and optimization, it is proved herein that the finite element based eigenanalysis constitutes a very efficient numerical tool. It is already exploited herein to devise two novel mode stirrers and study their behavior. These are proved more efficient from the most used in measurements Z-type stirrer. However, an extensive research is still required toward the exploitation of the eigenanalysis for the design of reverberation chambers to include multiple stirrers, as well as the presence of antennas and supporting tables or tripods.

## ACKNOWLEDGMENT

The Authors would like to thank Professors Niels Kuster and Quirino Balzano for their constructive comments during the preparation of this article. This research has been co-financed by the European Union (European Social Fund-ESF) and Greek national funds through the Operational Program "Education and Lifelong Learning" of the National Strategic Reference Framework (NSRF) — Research Funding Program: THALES. Inventing in knowledge society through the European Social Fund.

## APPENDIX A. EIGENFUNCTIONS OF A UNIFORMLY FILLED RECTANGULAR CAVITY

The analytical eigenfunctions of a uniformly filled rectangular cavity $a\times b\times c$ with PEC walls read [31, 32]:

For $TM_{mnl}$ modes:

$$E_z = A^e \sin\left(\frac{m\pi}{a}x\right)\sin\left(\frac{n\pi}{b}y\right)\cos\left(\frac{l\pi}{d}z\right) \tag{A1}$$

$$H_z = 0 \tag{A2}$$

$$E_x = -\frac{1}{k_c^2}\frac{m\pi}{a}\frac{l\pi}{d}A^e \cos\left(\frac{m\pi}{a}x\right)\sin\left(\frac{n\pi}{b}y\right)\sin\left(\frac{l\pi}{d}z\right) \tag{A3}$$

$$H_x = \frac{1}{k_c^2}j\omega\epsilon\frac{n\pi}{b}A^e \sin\left(\frac{m\pi}{a}x\right)\cos\left(\frac{n\pi}{b}y\right)\cos\left(\frac{l\pi}{d}z\right) \tag{A4}$$

$$E_y = -\frac{1}{k_c^2}\frac{n\pi}{b}\frac{l\pi}{d}A^e \sin\left(\frac{m\pi}{a}x\right)\cos\left(\frac{n\pi}{b}y\right)\sin\left(\frac{l\pi}{d}z\right) \tag{A5}$$

$$H_y = -\frac{1}{k_c^2}j\omega\epsilon\frac{m\pi}{a}A^e \cos\left(\frac{m\pi}{a}x\right)\sin\left(\frac{n\pi}{b}y\right)\cos\left(\frac{l\pi}{d}z\right) \tag{A6}$$

For $TE_{mnl}$ modes:

$$E_z = 0 \tag{A7}$$

$$H_z = A^h \cos\left(\frac{m\pi}{a}x\right)\cos\left(\frac{n\pi}{b}y\right)\sin\left(\frac{l\pi}{d}z\right) \tag{A8}$$

$$E_x = \frac{1}{k_c^2}j\omega\mu\frac{n\pi}{b}A^h \cos\left(\frac{m\pi}{a}x\right)\sin\left(\frac{n\pi}{b}y\right)\sin\left(\frac{l\pi}{d}z\right) \tag{A9}$$

$$H_x = -\frac{1}{k_c^2}\frac{l\pi}{d}\frac{m\pi}{a}A^h \sin\left(\frac{m\pi}{a}x\right)\cos\left(\frac{n\pi}{b}y\right)\cos\left(\frac{l\pi}{d}z\right) \tag{A10}$$

$$E_y = -\frac{1}{k_c^2}j\omega\mu\frac{m\pi}{a}A^h \sin\left(\frac{m\pi}{a}x\right)\cos\left(\frac{n\pi}{b}y\right)\sin\left(\frac{l\pi}{d}z\right) \tag{A11}$$

$$H_y = -\frac{1}{k_c^2}\frac{l\pi}{d}\frac{n\pi}{b}A^h \cos\left(\frac{m\pi}{a}x\right)\sin\left(\frac{n\pi}{b}y\right)\cos\left(\frac{l\pi}{d}z\right) \tag{A12}$$

where $k_c^2 = k_x^2 + k_y^2 = (\frac{m\pi}{a})^2 + (\frac{n\pi}{b})^2$.

## REFERENCES

1. IEC 61000-4-21-Electromagnetic Compatibility (EMC) — Port 4-21, "Testing and measurement techniques-reverberation chamber test methods, international electrotechnical commission (IEC)," Int. Std., CISPR/A and IEC SC 77B, IEC, Geneva, Switzerland, Apr. 2011.
2. Project for 2010–2013, "Institute of electronics, microelectronics and nanotechnology," http://www.iemn.univ-lille1.fr/en/home.html, 1992.

3. Kildal, P. S. and K. Rosengren, "Correlation and capacity of MIMO systems and mutual coupling radiation efficiency and diversity gain of their antennas: Simulation and measurements in reverberation chamber," *IEEE Communications Magazine*, Vol. 42, No. 12, 104–122, Dec. 2004.
4. Rosengren, K. and P. S. Kildal, "Study of distributions of modes and plane waves in reverberation chambers for the characterization of antennas in a multipath environment," *Microwave and Optical Technology Letters*, Vol. 30, No. 6, 386–391, Sep. 2001.
5. Clegg, J., A. C. Marvin, J. F. Dawson, and S. J. Porter, "Optimization of stirrer designs in a reverberation chamber," *IEEE Trans. on Electromagnetic Compatibility*, Vol. 47, No. 4, 824–832, Nov. 2005.
6. Bruns, C., "Three-dimensional simulation and experimental verification of a reverberation chamber," Ph.D., University of Fridericiana Karlsruhe, Germany, 2005.
7. Bruns, C. and R. Vahldieck, "A closer look at reverberation chambers 3-D simulation and experimental verification," *IEEE Trans. on Electromagnetic Compatibility*, Vol. 47, 612–626, Aug. 2005.
8. Karlsson, K., J. Carlsson, and P.-S. Kildal, "Reverberation chamber for antenna measurements: Modeling using method of moments, spectral domain techniques, and asymptote extraction," *IEEE Trans. on Antennas and Propagation*, Vol. 54, No. 11, 3106–3113, Nov. 2006.
9. Laermans, E., L. Knockaert, and D. De Zutter, "Two-dimensional method of moments modelling of lossless overmoded transverse magnetic cavities," *Journal of Computational Physics*, Vol. 198, 326–348, Elsevier, 2004.
10. Zhao, H. and Z. Shen, "Hybrid discrete singular convolution — Method of moments analysis of a 2-D transverse magnetic reverberation chamber," *IEEE Trans. on Electromagnetic Compatibility*, Vol. 52, No. 3, 612–619, Aug. 2010.
11. Zhao, H. and Z. Shen, "Memory-efficient modeling of reverberation chambers using hybrid recursive update discrete singular convolution-method of moments," *IEEE Trans. on Antennas and Propagation*, Vol. 60, No. 6, 2781–2789, Jun. 2012.
12. Gruber, M. E., S. B. Adrian, and T. F. Eibert, "A finite element boundary integral formulation using cavity Green's function and spectral domain factorization for simulation of reverberation chambers," *International Conference on Electromagnetics in Advanced Applications (ICEAA)*, 460–463, Sep. 9–13, 2013.
13. Yang, K. and A. E. Yilmaz, "An FFT-accelerated integral-equation solver for analyzing scattering in rectangular cavities," *IEEE Trans. on Microwave Theory and Techniques*, Vol. 62, No. 9, 1930–1942, Sep. 2014.
14. Zhao, H., "MLFMM-accelerated integral-equation modeling of reverberation chambers [open problems in CEM]," *IEEE Trans. on Antennas and Propagation*, Vol. 55, No. 5, 299–308, Oct. 2013.
15. Carlberg, U., P.-S. Kildal, and J. Carlsson, "Numerical study of position stirring and frequency stirring in a loaded reverberation chamber," *IEEE Trans. on Electromagnetic Compatibility*, Vol. 51, No. 1, 12–17, Feb. 2009.
16. Adardour, A., G. Andrieu, and A. Reineix, "Influence of a stirrer on the cavity modes within a reverberation chamber," *International Symposium on Electromagnetic Compatibility (EMC EUROPE)*, 1–4, Sep. 17–21, 2012.
17. Moglie, F., "Finite difference, time domain analysis convergence of reverberation chambers," *Proc. 15th Int. Zurich Symp. and Technical Exhibition on Electromagnetic Compatibility*, 223–228, Swiss Federal Inst. Technol. Zurich, Zurich, Switzerland, 2003.
18. Moglie, F. and V. M. Primiani, "Reverberation chambers: Full 3D FDTD simulations and measurements of independent positions of the stirrers," *IEEE International Symposium on Electromagnetic Compatibility (EMC)*, 226–230, Aug. 14–19, 2011.
19. Primiani, V. M. and F. Moglie, "Numerical determination of reverberation chamber field uniformity by a 3-D simulation," *International Symposium on Electromagnetic Compatibility (EMC EUROPE)*, 829–832, Sep. 26–30, 2011.
20. Lallechere, S., S. Girard, R. Vernet, P. Bonnet, and F. Paladian, "FDTD/FVTD methods and hybrid schemes applied to Reverberation chambers studies," *First European Conference on*

*Antennas and Propagation, EuCAP*, 1–6, Nov. 6–10, 2006.

21. Orjubin, G., E. Richalot, S. Mengue, M.-F. Wong, and O. S. Picon, "On the FEM modal approach for a reverberation chamber analysis," *IEEE Trans. on Electromagnetic Compatibility*, Vol. 49, No. 1, 76–85, Feb. 2007.
22. Orjubin, G., E. Richalot, O. S. Picon, and O. Legrand, "Chaoticity of a reverberation chamber assessed from the analysis of modal distributions obtained by FEM," *IEEE Trans. on Electromagnetic Compatibility*, Vol. 49, No. 4, 762–771, Nov. 2007.
23. Golias, N. A., T. V. Yioultsis, and T. D. Tsiboukis, "Vector complex eigenmode analysis of microwave cavities," *IEEE Proc. — Microw. Antennas Propag.*, Vol. 142, 457–461, Dec. 1995.
24. Zekios, C. L., P. C. Allilomes, C. S. Lavranos, and G. A. Kyriacou, "A three dimensional finite element eigenanalysis of reverberation chambers," *EMC Europe Workshop 2009 — Materials in EMC Applications*, 129–132, Athens, Greece, Jun. 11–12, 2009.
25. Zekios, C. L., P. C. Allilomes, and G. A. Kyriacou, "A finite element eigenanalysis of arbitrary loaded cavities including conductor losses," *32nd ESA Antenna Workshop on Antennas for Space Applications*, Noordwijk, The Netherlands, Oct. 5–8, 2010.
26. Press, W. H., B. P. Flannery, S. A. Teukolsky, and W. T. Vetterling, *Numerical Recipes in FORTRAN 77: The Art of Scientific Computing*, Cambridge University Press, 1992.
27. Zekios, C. L., P. C. Allilomes, and G. A. Kyriacou, "On the evaluation of eigenmodes quality factor of large complex cavities based on a PEC linear finite element formulation," *Electronics Letters*, Vol. 48, No. 22, 1399–1401, Oct. 2012.
28. Zhu, Y. and A. C. Cangellaris, *Multigrid Finite Element Methods for Electromagnetic Field Modeling*, Wiley Interscience, 605 Third Avenue, New York, 2006.
29. Reddy, C. J., M. D. Deshpande, C. R. Cockrell, and F. B. Beck, "Finite element method for eigenvalue problems in electromagnetics," NASA Technical Paper 3485, Dec. 1994.
30. Lehman, T. H., "A statistical theory of electromagnetic fields in complex cavities," Interaction Note 494, Sandia Labs, May 1993.
31. Harrington, R. F., *Time-harmonic Electromagnetic Fields*, IEEE Press, John Wiley and Sons, Inc., 605 Third Avenue, New York, 2001.
32. Jackson, J. D., *Classical Electrodynamics*, 3rd edition, Wiley, New York, 1999
33. Balanis, C. A., *Advanced Engineering Electromagnetics*, John Wiley and Sons, Inc., 605 Third Avenue, New York, 1989.
34. Saad, Y., *Iterative Methods for Sparse Linear Systems*, 2nd Edition, Society for Industrial and Applied Mathematics, 2000.
35. SALOME, http://www.salome-platform.org/, 2005.
36. FEniCS, http://fenicsproject.org/, 2013.
37. The HDF group, http://www.hdfgroup.org/, 2013.
38. Extensible Markup Language (XML), http://en.wikipedia.org/wiki/XML, 2014.
39. Godfrey, E. A., "Effects of corrugated walls on the field uniformity of reverberation chambers at low frequencies," *IEEE International Symposium on Electromagnetic Compatibility (EMC)*, Vol. 1, 23–28, 1999.